

NASA
TP
1358
c.1

NASA Technical Paper 1358

LOAN COPY: RETU
AFWL TECHNICAL L
KIRTLAND AFB, N

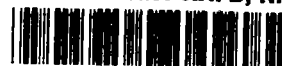


Theoretical Evaluation of High-Speed Aerodynamics for Arrow-Wing Configurations

Samuel M. Dollyhigh

JANUARY 1979

NASA



NASA Technical Paper 1358

Theoretical Evaluation of High-Speed Aerodynamics for Arrow-Wing Configurations

Samuel M. Dollyhigh
*Langley Research Center
Hampton, Virginia*



National Aeronautics
and Space Administration

**Scientific and Technical
Information Office**

1979

SUMMARY

A limited study of the use of theoretical methods to calculate the high-speed aerodynamic characteristics of arrow-wing supersonic cruise configurations has been conducted. The study included correlations of theoretical predictions with wind-tunnel data at Mach numbers from 0.80 to 2.70, examples of the use of theoretical methods to extrapolate the wind-tunnel data to full-scale flight condition, and presentation of a typical supersonic data package for an advanced supersonic transport application prepared using the theoretical methods. A brief description of the methods and their application is given.

Basically, three theoretical methods were used to calculate high-speed aerodynamic characteristics. These methods were as follows: (1) a group of in-house Langley Research Center analysis programs, (2) a computational system for aerodynamic design and analysis of supersonic aircraft, and (3) a generalized vortex-lattice program. The first two methods are purely supersonic methods while the last applies to both subsonic and supersonic speeds. In general, all three methods had excellent correlation with wind-tunnel data at supersonic speeds for drag and lift characteristics and fair to poor agreement for pitching-moment characteristics. The vortex-lattice program had excellent correlation up to a lift coefficient of 0.3 with wind-tunnel data at subsonic speeds for lift and pitching-moment characteristics and fair agreement for drag characteristics.

INTRODUCTION

Rapid advances in computational equipment and numerical techniques have led to increasing reliance on theoretical methods for generation of aerodynamic performance estimates for use in airplane design studies. In addition to their direct design features, modern analytic methods provide the opportunity to study a wide range of candidate configurations in the selection of a baseline design and are of great value in the conduct of trade studies involving other aspects of airplane design. An important feature of the computer methods utilized is the ability to represent all the major airplane components and to account for mutual aerodynamic interference, a factor of real significance at supersonic speeds.

Analytic methods also serve to supplement wind-tunnel data by providing a means for estimating the effects of configuration changes on aerodynamic performance in such a way that interference effects are taken into account. Aerodynamic estimates made by applying increments to the normally sparse array of wind-tunnel data for complex configurations in the absence of interference considerations can be misleading. Another way in which analytic methods aid the experimental process is by providing an extrapolation of aerodynamic coefficients from wind-tunnel to flight conditions.

The object of this report is to present a description of some of the methods used at the Langley Research Center and to assess their ability to provide estimates of aerodynamic performance by means of correlations with wind-tunnel data for a representative supersonic cruise configuration. In addition, examples of the use of analytic methods for correction and extrapolation of wind-tunnel data are given and a typical aerodynamic data package as used in design studies is discussed.

The high-speed experiment-theory correlation covers the Mach number range from 0.80 to 2.70. It was desirable to do a correlation at lower Mach numbers ($M = 0.40$ to 0.60), but no experimental data were available for the configuration. A typical data-base problem also exists in the supersonic region where there is a data gap between Mach 1.20 and 2.30. The configuration on which the experiment-theory correlation and extrapolation to full scale is performed is the SCAT 15-F-9898, which was designed and tested in the late 1960's. The configuration had a design Mach number of 2.70 and a 74° swept warped wing with a reflexed trailing edge and four engine nacelles mounted below the reflexed portion of the wing. The wind-tunnel test data for this configuration are presented in the appendix. The typical aerodynamic data package is for a current in-house reference supersonic aircraft designated AST-105. The AST-105 is the latest in-house study configuration used to measure and understand the benefits of advanced technology from the Supersonic Cruise Aircraft Research (SCAR) program on this type of airplane.

SYMBOLS

The measurements and calculations of this investigation were made in the U.S. Customary Units. Results are presented in both SI and U.S. Customary Units except in the computer printout of the appendix, where only U.S. Customary Units are used for dynamic pressure and Reynolds number per foot. (A waiver has been granted for this exception.)

BL buttock line

$C_{A,n}$ nacelle-on-wing interference axial-force coefficient, $\frac{\text{Axial force}}{qS}$

C_D drag coefficient, $\frac{\text{Drag}}{qS}$

$C_{D,f}$ skin-friction drag coefficient

$C_{D,i}$ induced-drag (drag-due-to-lift) coefficient

$C_{D,min}$ minimum drag coefficient

$C_{D,o}$ subsonic profile-drag coefficient

$C_{D,r}$ roughness-drag coefficient

$C_{D,w}$	zero-lift wave-drag coefficient
C_L	lift coefficient, $\frac{\text{Lift}}{qS}$
$C_{L,MD}$	lift coefficient for minimum drag
C_m	pitching-moment coefficient, $\frac{\text{Pitching moment}}{qS\bar{c}}$
$C_{m,0}$	pitching-moment coefficient at $C_L = 0$
$C_{N,n}$	nacelle-on-wing interference normal-force coefficient, $\frac{\text{Normal force}}{qS}$
c	wing chord, cm (in.)
\bar{c}	wing mean aerodynamic chord, cm (in.)
$\frac{\partial C_m}{\partial C_L}$	longitudinal stability parameter at $C_L = 0$
i_t	horizontal-tail incidence angle with respect to wing reference plane, deg
K_1, K_2	drag-due-to-lift factors (see fig. 16), $C_{D,i} = K_1 + K_2(C_L - C_{L,MD})^2$
L/D	lift-drag ratio
$(L/D)_{\max}$	maximum lift-drag ratio
M	free-stream Mach number
q	free-stream dynamic pressure, Pa (lb/ft ²)
S	wing reference area, m ² (ft ²)
x	longitudinal station, rearward from nose, cm (in.)
α	angle of attack, deg
$\delta_{L,6}$	deflection of flap on wing tip with deflection measured normal to leading edge (positive for leading edge down), deg
Λ	leading-edge sweep angle, deg

DESCRIPTION OF THEORETICAL METHODS USED

The theoretical methods used to evaluate aerodynamic forces and moments on complete airplane configurations consist of a set of compatible computer codes that utilize linear theory. The drag analysis has been performed as illustrated in figure 1. At subsonic speeds, an induced-drag coefficient which includes interference effects between wing and nacelles is added to the skin-friction coefficient and an empirical profile-drag or form-drag coefficient which is expressed as a percentage of the skin-friction coefficient. At supersonic speeds, drag due to lift, which includes different degrees (depending on the method used) of interference effects between components, is added to the skin-friction and wave-drag coefficients. Differences in how interference effects are handled are treated as each method is discussed. This composite system of supersonic drag analysis which mixes far-field and near-field methods is discussed in reference 1. The lift and pitching-moment characteristics are computed simultaneously with the induced-drag or drag-due-to-lift calculations and also include different degrees (depending on the method used) of interference effects between components. All the computer codes employed require a numerical description of the configuration that can be defined from a standard geometry deck. A description of the geometry modeling technique is presented in reference 2. The use of a standard geometry format to calculate both subsonic and supersonic aerodynamic characteristics is very desirable. The individual methods employed in the calculation of aerodynamic characteristics are discussed subsequently.

Skin Friction

Both wind-tunnel and flight skin-friction drag coefficients at subsonic and supersonic speeds have been computed using the T' method described in reference 3. The configuration drag coefficient is computed by representing the various configuration components by appropriate wetted areas and reference lengths assuming smooth-flat-plate, adiabatic-wall, boundary-layer conditions. For wind-tunnel test conditions, the drag is computed for a given Mach number, stagnation temperature, and Reynolds number per unit length. For flight conditions, the drag is computed for a given Mach number and altitude for a standard hot day (283 K (10° C)). Transition location from laminar to turbulent boundary is specified for wind-tunnel skin friction, and this transition is assumed to occur at the leading edge of each component for full-scale flight conditions. Configuration components, such as the wing or tail, which may exhibit significant variations in reference length are further subdivided into strips for a more accurate determination of the friction drag.

Subsonic Profile Drag

In addition to the subsonic friction drag, there is a profile or separation drag due to flow detachment along the afterbody of airfoils or fusiform bodies. This component does not lend itself to theoretical analysis and is evaluated by the empirical methods of reference 4. Each component is assigned a form factor which expresses the profile drag as a percentage of skin friction (usually from 3 to 5 percent).

Zero-Lift Wave Drag

The far-field wave-drag program uses the supersonic area-rule concept to compute the zero-lift wave drag of an arbitrary configuration as described in reference 5. Equivalent bodies of revolution are calculated by passing a number of cutting planes inclined at the Mach angle through the configuration for several different airplane azimuth angles. The wave drag of each equivalent body is determined from the von Karman slender-body theory, which relates the wave drag to the free-stream conditions and the equivalent-body area distribution. The discrete equivalent-body wave-drag values are integrated around the configuration and averaged to obtain overall wave drag.

Nacelle Interference Effects

Interference loads imposed on the wing by the four nacelles located below the wing at the trailing edge have been computed using a modified version of the method described in reference 6. The program uses linearized theory as corrected for the presence of finite shocks according to reference 7 to compute the loads imposed on a warped-wing surface by nacelles located either above or below the wing. For this study, the author of reference 6 provided an unpublished modified program which allows for the lower supersonic Mach number cases in which the interference flow field from the nacelles simultaneously affects the upper and lower wing surfaces. These nacelle-on-wing interference coefficients are used directly in the lift analysis discussed in the following section to obtain the lift, drag due to lift, and pitching-moment characteristics with the nacelle interference effects included.

Lift Analysis

The wing lifting characteristics, drag due to lift, and pitching-moment behavior were computed using the linear-theory method described in reference 8. The method breaks an arbitrary planform arrangement into a mosaic of "Mach box" rectilinear elements which are assumed to lie in the horizontal ($z = 0$) plane. These grid elements are then employed to numerically evaluate the linear-theory integral equation which relates the lifting pressure at a given field point to the wing-surface slopes in the region of influence of that field point. The overall force coefficients for the camber surface at incidence are obtained by integrating the computed pressure distribution over the wing surface. This solution is combined using a superposition technique with a flat-wing solution per unit angle of attack to obtain the variation of the force coefficient with angle of attack. The nacelle interference effects previously discussed are incorporated with the lift, drag due to lift, and pitching-moment characteristics computed by this method.

The previously described methods to calculate skin friction, subsonic profile drag, zero-lift wave drag, nacelle interference effects, and the lift analysis are those programs that are collectively referred to as the Langley programs.

Generalized Vortex-Lattice Method

A generalized vortex-lattice program identified as VORLAX was used to calculate the subsonic induced drag and was used as one of the three methods to calculate supersonic drag due to lift. The VORLAX method presented in reference 9 is applicable to complete airplane configurations at both subsonic and supersonic flight conditions. The computational capabilities of the program include determination of (1) surface-pressure or net-load coefficient distribution, (2) aerodynamic force and moment coefficients, (3) surface warp (camber and twist) design in order to support a given pressure distribution, (4) longitudinal and lateral stability derivatives, (5) ground and wall interference effects, and (6) flow-field properties. Both symmetric and asymmetric configurations and/or flight conditions can be considered. Assumptions basic to the method require attached flow, small perturbations, all subsonic or supersonic (no mixed transonic) flow, straight Mach lines, and rigid vortex wake. Techniques for simulating nonzero-thickness lifting surfaces and fusiform bodies are also implemented.

The basic element of the method is the swept horseshoe vortex, whose trailing legs have both bound and free segments. Associated with each horseshoe vortex is a control point at which the local boundary condition is applied. The horseshoe vortices provide a velocity field which is used to generate the coefficients of a system of linear equations relating the unknown vortex strengths to the appropriate boundary conditions. Solution of this system of linear equations results in the calculation of local flow velocities, pressure coefficients, and the configuration aerodynamic characteristics. If the design mode is desired, a straightforward matrix multiplication is used to determine the surface slope distribution required to support the given pressure distribution.

For the experiment-theory correlation section of this report, the configuration was represented to the VORLAX program as cambered planar surfaces with engine nacelles (no wing thickness or fuselage volume). Induced drag or drag due to lift, lift, and pitching-moment coefficients which included wing-nacelle interference were calculated. Skin friction plus profile drag and skin friction plus wave drag were added to the VORLAX results to obtain the respective subsonic and supersonic drag polars. Skin friction, profile drag, and wave drag were calculated using the previously discussed methods.

Supersonic Design and Analysis System (Boeing Program)

The Boeing Company has extended and combined all the programs previously discussed except the VORLAX program into an integrated system of computer programs. (See refs. 10 to 12.) The extensions to the analysis methods are addition of a near-field (thickness-pressure) wave-drag program, an improved lift-analysis program which provides for separate modeling of fuselage lift and includes the interference of wing lift on nacelles, and the addition of pressure-limiting terms in the lifting-pressure programs to constrain the linear-theory solution. Brief descriptions of these extensions are given in the sections which follow.

Near-Field Wave Drag

The near-field wave-drag program computes zero-lift thickness-pressure distributions for an arbitrary wing-body-nacelle-empennage configuration. The distributions are integrated over the cross-sectional areas of the configuration to obtain the resultant drag force. The Whitham near-field method is used to define pressure distributions propagating from the fuselage or nacelles and superposition is used to calculate the interference drag terms associated with the pressure field from a component acting on the surfaces of the other components. The following interference terms are included: wing on fuselage, fuselage on wing, nacelle on wing, wing on nacelle, fuselage on nacelle, nacelle on fuselage, and nacelle on nacelle. The near-field method is particularly useful in studying pressure distributions.

Lift Analysis

The lift-analysis program uses the same basic technology used in the previously discussed individual programs, but includes the following additional features: the effect of fuselage upwash field on the wing-canard, the effect of wing downwash on the fuselage lift distribution, and the effects of the wing pressure field acting on the nacelles. The fuselage is assumed to be a body of revolution and the local surface angles of attack of the wing-canard are increased by the fuselage upwash values. If the area growth of the fuselage is asymmetric (e.g., a high or low wing configuration), an approximate method is used to compute the asymmetric fuselage pressure field using the Whitham technique (ref. 7). In addition, an optional pressure-limiting feature is provided. The permissible level of upper-surface pressure coefficient that is calculated by linear theory may be set to a specified fraction of vacuum.

For the experiment-theory correlation section of this report, the Boeing program was one of three methods used to calculate supersonic drag due to lift, lift, and pitching-moment characteristics of the configuration. Skin-friction and far-field wave-drag coefficients were added to the drag due to lift to determine the drag polars using this method.

COMPARISON OF THEORETICAL AND EXPERIMENTAL RESULTS

An experiment-theory correlation was performed on the SCAT 15-F-9898 configuration in the Mach number range from 0.80 to 2.70. Drawings of the complete model configuration are shown in figure 2. The configuration had a design Mach number of 2.70 and a 74° swept warped wing with a reflexed trailing edge and four engine nacelles mounted below the reflexed portion of the wing. Because of the desire to do a correlation for a model-component buildup, the experiment-theory correlation was carried out on two slightly different configurations. The configuration for the Mach 2.30 to 2.70 range had component buildup data available for a configuration with a 65° leading-edge sweep on the outer wing panel. The configuration for Mach 0.80 to 1.20 had an extended outer wing panel which had a leading-edge sweep angle of 60° and included leading-edge flaps. (See fig. 2(b).) No model-component buildup was available at the lower

Mach numbers. Details of the wind-tunnel test, corrections, and tabulated results are given in the appendix.

Figure 3 presents the experiment-theory correlation at Mach numbers of 0.80 and 0.90. Theory in this correlation is the VORLAX program results for the configuration represented as a cambered planar surface plus skin-friction and form-drag coefficients. The VORLAX program results include wing-nacelle interference. There is excellent agreement, up to a lift coefficient of about 0.3, between theory and experiment for lift and pitching-moment characteristics, but only fair agreement for drag-coefficient characteristics. Although it was not done, it is believed that representing the fuselage volume and planar surface thicknesses to the VORLAX program would improve the drag correlation.

The correlation between theory and experiment at Mach 1.20 is presented in figure 4 for the configuration with the wing-tip leading-edge flap (see fig. 2(b)) deflected 0° , 10° , and 20° . The theories shown are the results of the Boeing program and the individual supersonic programs collectively referred to as the Langley programs. The VORLAX program did not converge on a result at Mach 1.20. The Langley programs did an excellent job of predicting the aerodynamic characteristics with flaps undeflected, while the Boeing program did not predict quite as well. Experimental aerodynamic effects due to deflection of the leading-edge flap are small and, except for drag, are predicted to be so. The Boeing program does a good job of predicting the drag effects and the Langley program overpredicts the effect on drag coefficient of deflecting the flap, especially for the 20° flap deflection. However, linear-theory programs are not expected to do very well at this high a deflection angle.

Figures 5 to 7 show the correlation between theory and experiment obtained at Mach numbers of 2.30 and 2.70 for the three theoretical methods used. The VORLAX results are shown as four discrete calculated points instead of a curve because a sufficient number of calculations were not performed to define the drag characteristics completely. The theoretical results are carried to as high a lift coefficient as that generally available for the experimental results; however, the area of primary interest is usually lift coefficients from 0 to approximately 0.15.

The data in figures 5 to 7 are for a component buildup of the SCAT 15-F-9898 configuration. Figure 5 presents data for the wing-fuselage, the four engine nacelles are added in figure 6, and data for the complete configuration are presented in figure 7. The correlation between theory and experiment is excellent for drag and lift-coefficient characteristics for all three theoretical methods and for any combination of components. The Boeing program defines the drag polars better at the higher lift coefficients; however, there is little difference at the lift coefficients of interest. In general, the pitching-moment characteristics are not well predicted by any of the three theoretical methods, but the Langley programs tend to be reasonably close to predicting the zero-lift pitching-moment coefficient.

CORRECTION TO FULL SCALE

The major corrections of wind-tunnel data to full-scale airplane conditions are the skin-friction-coefficient correction for Reynolds number differences and the drag-coefficient correction due to geometry differences between the model and airplane. The drag-coefficient correction due to differences between the model and airplane is usually limited to a wave-drag correction for model geometry changes necessary to accommodate the balance and sting if the model is properly constructed. Proper construction entails not only representing the airplane geometry as accurately as possible, but also scaling the inlet diverter height so that airplane spillage is duplicated. In addition to the major corrections, a drag increment associated with the surface roughness due to manufacturing techniques is estimated to be approximately 3 and 6 percent of the skin-friction coefficient at subsonic and supersonic speeds, respectively. If the wind-tunnel data are not corrected for the drag caused by the grit of the transition strip, a drag increment due to grit roughness may be determined from the drag increment between a grit-on run and a grit-off run. This grit-on-grit-off drag increment must be corrected to account for the difference between turbulent conditions and the additional laminar-flow region associated with grit off. Sublimation photographs are necessary to determine the additional region of laminar flow. This information was available to correct the SCAT 15-F-9898 data; however, if this type of data is not available, the method of reference 13 may be used to predict the drag of roughness elements used in boundary-layer trips. In addition to the foregoing corrections, operational items such as air conditioning and engine-bleed drag are sometimes included in the extrapolation to full scale. These operational items are not included in the aerodynamic extrapolation to full scale performed herein.

The extrapolation of wind-tunnel data to full-scale flight conditions presented in figure 8 is for the SCAT 15-F-9898 at the design Mach number of 2.70. Drag-coefficient increments applied to the wind-tunnel data are presented in table I. The airplane skin-friction coefficient was calculated for an altitude of 18 288 m (60 000 ft) assuming a standard atmosphere, a surface emittance of 0.8, and a surface sand grain roughness of $7.6 \mu\text{m}$ (2.5×10^{-5} ft). The drag increment due to surface roughness (rivet heads, gaps, etc.) and miscellaneous surface defects was assumed to be 6 percent of the airplane skin-friction drag. Model-airplane geometry differences due to model distortion necessary to insert a balance and sting resulted in a wave-drag increment to be applied to the data. The wetted-area difference due to model distortion was accounted for in the respective skin-friction calculations. The grit drag increment was calculated by the method previously discussed. As seen in figure 8, applying these drag increments to the wind-tunnel data results in an extrapolated airplane $(L/D)_{\text{max}}$ of 9.6 compared with 7.2 for the wind-tunnel test for the baseline drag polar. Depending on the method used to trim the aircraft (i.e., center-of-gravity control by pumping fuel or by horizontal tail deflection), a trim drag increment may or may not need to be applied to the drag characteristics. Also, it was assumed that the wind-tunnel tests correctly modeled the airplane pitching-moment and lift characteristics, so no corrections to these were necessary.

TYPICAL SST APPLICATION

Theoretical lift, drag, and pitching-moment characteristics of the AST-105 configuration (fig. 9) have been computed for Mach numbers from 1.10 to the 2.62 cruise condition. In addition, the horizontal-tail incidence angle required for maximum configuration performance has been calculated and maintained at all Mach numbers. The analysis has utilized the individual methods (Langley programs) that have been previously discussed. The data package presented is typical of that used for supersonic aerodynamics in preliminary sizing and performance evaluation. Insofar as possible, this information is generated in equation form or curve-fit expressions for ease of handling in the sizing and performance programs.

The design Mach 2.62 equivalent-area distributions developed by the wave-drag program for both the fuselage and the complete configuration are shown in figure 10. The smoothness of this curve indicates that wave drag has been minimized at the cruise Mach number. Any "bumps" in this curve indicate a potential to improve the drag characteristics by applying the area rule to the configuration. The configuration wave-drag variation with Mach number is presented in figure 11. The skin-friction analysis along the desired Mach number-altitude flight profile is presented in figure 12 where both climb and cruise conditions are illustrated. Table II presents component wetted areas and skin-friction coefficients for three representative Mach number-altitude combinations. The configuration roughness-drag increment was assumed to be 6 percent of the friction drag for the Mach 2.62 cruise condition. For the lower Mach number, the ratios of roughness drag to skin friction increase as Mach number is lowered toward 1. These ratios are based on estimates by aircraft manufacturers for similar configurations. The resulting variation of roughness-drag coefficient with Mach number is shown in figure 13.

Interference loads imposed on the wing by the four nacelles located below the wing at the trailing edge have been computed by the nacelle interference program and are summarized in figure 14 as normal- and axial-force coefficients. The interference effects are used directly in the drag-due-to-lift analysis to obtain the lift, drag due to lift, and pitching-moment characteristics with the nacelle interference effects included. If it is assumed that trim requirements for the configuration are met through suitable center-of-gravity control, then airplane performance is optimized by flying the configuration with the horizontal tail oriented to maximize lift-drag ratio at each Mach number. Figure 15 presents the results of a study to determine the required tail incidence angle. As the figure indicates, the configuration $(L/D)_{\max}$ is not overly sensitive to tail setting. Table III presents the horizontal-tail incidence angles used to maximize the overall aerodynamic characteristics presented in the figures. The configuration drag-due-to-lift parameters with tail settings as indicated in table III are presented in figure 16.

The overall aerodynamic characteristics for the AST-105 configuration are summarized in figures 17 to 21. Typical drag polars obtained by combining the various zero-lift drag items with the drag-due-to-lift characteristics (as shown in fig. 1(b)) are presented in figure 17. The associated lift curves are shown in figure 18 while the variation of $(L/D)_{\max}$ with Mach number derived from

these lift and drag characteristics is summarized in figure 19. A start-of-cruise value of 9.0 is indicated by the analysis.

The pitching-moment characteristics are presented in figures 20 and 21. The pitching-moment characteristics have been computed using the horizontal-tail incidence angles previously discussed and with center-of-gravity locations typical of an actual mission profile for the AST-105 configuration. Thus both ascent and descent pitching-moment characteristics are indicated.

CONCLUDING REMARKS

A limited study of the use of theoretical methods to calculate the high-speed aerodynamic characteristics of arrow-wing supersonic cruise configurations has been conducted. The study included correlations of theoretical predictions with wind-tunnel data at Mach numbers from 0.80 to 2.70, examples of the use of theoretical methods to extrapolate the wind-tunnel data to full-scale flight conditions, and an illustration of a typical supersonic data package for an advanced supersonic transport application prepared using the theoretical methods. A brief description of the methods and their application is given.

Basically, three theoretical methods were used to calculate the high-speed aerodynamic characteristics. These methods were as follows: (1) a group of in-house Langley Research Center analysis programs, (2) a computational system for aerodynamic design and analysis of supersonic aircraft (Boeing program), and (3) a generalized vortex-lattice program (VORLAX). The first two methods are purely supersonic methods while the last applies to both subsonic and supersonic speeds. In general, all three methods had excellent correlation with wind-tunnel data at supersonic speeds for drag and lift characteristics and fair to poor agreement with pitching-moment characteristics. The VORLAX program had excellent correlation up to a lift coefficient of 0.3 with wind-tunnel data at subsonic speeds for lift and pitching-moment characteristics and fair agreement in drag characteristics.

Langley Research Center
National Aeronautics and Space Administration
Hampton, VA 23665
November 3, 1978

APPENDIX

WIND-TUNNEL DATA

The wind-tunnel data used in this report were taken from references 14 and 15. Complete details of the wind-tunnel tests, which consisted of many more model configurations than reported herein, are given in these references.

Drawings of the model configuration used for comparison of theoretical and experimental results are shown in figure 2. Detailed geometric characteristics of the baseline (65° tip) model are presented in table AI. The model scale was 0.015, which represents a full-scale supersonic transport aircraft configuration approximately 91.44 m (300 ft) in length.

The model incorporated a slender cambered body with a 74° swept wing planform which was designed for a cruise lift coefficient of 0.08 at a Mach number of 2.70. The wing had a subsonic leading edge except in the region of the tip where the leading-edge angle was decreased to 65° on the basic configuration and 60° on the subsonic-transonic modified configuration. The modified outer wing panel was equipped with movable leading-edge flaps (fig. 2(b)). Details of the remaining components are available in references 13 and 14.

A small horizontal tail was mounted aft on the fuselage to provide longitudinal pitch control. Two vertical tails were mounted on the outboard wing panels for directional stability and to improve the airflow in the region of the wing tip. A fuselage-mounted vertical tail and a ventral fin were also included to provide directional control.

Four engine nacelles were located below the wing near the wing trailing edge to simulate engine installation. The wing trailing edge was reflexed upward in the region of the engine nacelles in order to essentially cancel the lift interference from the nacelles and to improve the drag-interference effects of the wing-nacelle combination at cruise conditions.

Tabular data that are used in this report are from references 13 and 14. From Mach 0.80 to 1.20 boundary-layer transition to turbulent flow conditions was fixed at 3.05 cm (1.2 in.) aft of the nose of the fuselage and streamwise 1.52 cm (0.60 in.) from the leading edge of all external surfaces and on the inside of the engine nacelles. At conditions of Mach 2.30 and 2.70, the fuselage transition remained the same and the transition was fixed at 1.02 cm (0.40 in.) from the leading edge of all external surfaces and on the inside of the engine nacelles. The experimental data in the main body of this report are plots of the referenced data, except for drag characteristics at Mach 1.20. The tabular data for Mach 1.20 had a constant nacelle-base-drag-coefficient correction of 0.0021 applied to drag results. The correction should have varied linearly from 0.0016 at $C_L = -0.05$ to 0.0022 at $C_L = 0.42$. The linearly varying correction was applied to the plotted data, otherwise the data were used as presented in the following table:

APPENDIX

Run	Mach number	Configuration
8	0.80	W _{60,tip} BEVH $\delta_{L,6} = 0^\circ$
3	.90	
4	1.20	
10	1.20	
16	1.20	
93	2.30	
95	2.70	
146	2.30	W _{65,tip} BE $\delta_{L,6} = 10^\circ$
148	2.70	BE $\delta_{L,6} = 20^\circ$
150	2.30	B
152	2.70	B

The results of the wind-tunnel tests are presented as follows:

SCAT 15-F

TEST 503 RUN 4 MACH 1.200

POINT	TIME	Q	BETA	ALPHA	CN	CA	CM	CL	CD	L/D	CDX	CDA	CDI	R/FT
90	1.200	417.53	.00	-5.62	-.1194	-.01139	.0362	-.1177	.01792	-5.91	.00111	.00210	.0010	2.00
91	1.200	417.58	.01	-4.25	-.0631	-.01361	.0274	-.0619	.01514	-4.00	.00114	.00210	.0010	2.00
92	1.200	417.68	.01	-3.50	-.0301	-.01483	.0221	-.0297	.01355	-2.15	.00116	.00210	.0010	2.00
93	1.201	417.66	.01	-2.79	-.0006	.01582	.0170	.0002	.01273	.01	.00117	.00210	.0010	2.00
94	1.201	417.71	.01	-2.11	.0261	.01668	.0124	.00267	.01261	2.12	.00118	.00210	.0010	2.00
95	1.201	417.71	.01	-1.61	.0534	.01735	.0079	.0534	.01293	4.16	.00118	.00210	.0010	2.00
96	1.203	417.63	.01	-.73	.0789	.01784	.0040	.0791	.01373	5.76	.00119	.00210	.0010	2.00
97	1.203	417.63	.01	-.02	.1077	.01324	-.0006	.1077	.01510	7.13	.00120	.00210	.0010	2.00
98	1.203	417.63	.01	.69	.1369	.01951	-.0052	.1367	.01705	8.02	.00123	.00210	.0010	2.00
99	1.203	417.63	.01	1.34	.1662	.01974	-.0101	.1657	.02351	9.45	.00126	.00210	.0010	2.00
100	1.203	417.63	.01	2.11	.1894	.01929	-.0159	.1985	.02909	10.12	.00130	.00210	.0010	2.00
101	1.200	417.66	.01	2.89	.2376	.02027	-.0219	.2363	.02909	11.00	.00132	.00210	.0010	2.00
102	1.200	417.63	.01	3.69	.2755	.02144	-.0272	.2735	.03597	12.60	.00131	.00210	.0010	2.00
103	1.200	417.63	.01	4.50	.3160	.02293	-.0318	.3132	.04456	14.03	.00133	.00210	.0010	2.00
104	1.203	417.63	.01	5.35	.3564	.02452	-.0356	.3525	.05455	16.46	.00145	.00210	.0010	2.00
105	1.200	417.66	.01	6.19	.3941	.02612	-.0387	.3900	.06535	19.95	.00137	.00210	.0010	2.00
106	1.200	417.60	.01	7.05	.4339	.02756	-.0416	.4272	.07792	24.48	.00140	.00210	.0010	2.00
107	1.200	417.66	.01	7.94	.4746	.03006	-.0442	.4659	.09224	30.05	.00144	.00210	.0010	2.00
108	1.200	417.60	.01	8.19	.4879	.03076	-.0452	.4786	.09897	34.94	.00150	.00210	.0010	2.00
109	1.201	417.71	.00	-5.66	-.1223	-.01128	.0368	-.1206	.02019	-5.97	.00112	.00210	.0010	2.00

TEST 503 RUN 3 MACH .900

POINT	TIME	Q	BETA	ALPHA	CN	CA	CM	CL	CD	L/D	CDX	CDA	CDI	R/FT
67	.901	359.40	.00	-5.74	-.1301	-.00870	.0337	-.1285	.01987	-6.47	.00027	.00080	.0010	1.99
68	.903	357.44	.00	-4.25	-.0675	-.01098	.0265	-.0664	.01417	-4.69	.00029	.00080	.0010	1.99
69	.903	357.50	.00	-3.64	-.0416	-.01195	.0233	-.0407	.01276	-3.19	.00027	.00080	.0010	2.00
70	.901	359.01	.00	-2.52	-.0102	.01302	.0191	-.0096	.01173	-.02	.00024	.00080	.0010	2.00
71	.903	357.77	.01	-2.24	.0150	.01374	.0154	.0155	.01134	1.37	.00031	.00080	.0010	2.00
72	.901	357.76	.01	-1.51	.0435	.01446	.0119	.0439	.01150	3.82	.00032	.00080	.0010	2.00
75	.901	357.88	.01	-.50	.0673	.01494	.0092	.0676	.01198	5.64	.00033	.00080	.0010	2.00
76	.900	357.65	.01	-.20	.0903	.01504	.0067	.0903	.01293	6.99	.00034	.00080	.0010	2.00
77	.903	357.72	.01	.45	.1181	.01508	.0038	.1179	.01429	8.25	.00034	.00080	.0010	2.00
78	.903	357.65	.01	1.17	.1448	.01510	.0011	.1445	.01626	9.80	.00034	.00080	.0010	2.00
79	.903	357.71	.01	1.95	.1803	.01529	-.0030	.1797	.01661	11.16	.00036	.00080	.0010	2.00
80	.900	357.71	.01	2.65	.2146	.01589	-.0081	.2136	.02597	12.91	.00037	.00080	.0010	2.00
81	.903	357.47	.01	3.38	.2505	.01658	-.0123	.2491	.02950	14.44	.00039	.00080	.0010	2.00
82	.900	357.68	.00	4.19	.2912	.01766	-.0167	.2891	.03707	17.00	.00042	.00080	.0010	2.00
83	.903	357.59	.00	5.01	.3332	.01894	-.0201	.3303	.04616	20.61	.00044	.00080	.0010	2.00
84	.900	357.49	.00	5.83	.3740	.02046	-.0223	.3700	.05657	24.54	.00046	.00080	.0010	2.00
85	.903	357.65	.00	6.70	.4171	.02218	-.0238	.4116	.06801	29.97	.00046	.00080	.0010	2.00
86	.903	357.54	.00	7.54	.4576	.02386	-.0247	.4505	.08190	35.50	.00054	.00080	.0010	2.00
87	.903	357.72	.01	8.51	.5064	.02616	-.0259	.4969	.09902	50.02	.00057	.00080	.0010	2.00
88	.903	357.47	.01	9.34	.5518	.02858	-.0297	.5398	.11509	60.65	.00058	.00080	.0010	2.00
89	.903	357.77	.00	-5.73	-.1312	-.00870	.0338	-.1297	.01985	-6.50	.00027	.00080	.0010	2.00

APPENDIX

SCAT 15-F

TEST 503														FLIN 8		MACH .800	
POINT	MIN-	Q	BETA	ALPHA	CN	CA	CM	CL	CD	L/D	CDC	CDB	CPI	R/FT			
172	.7902	329.97	.01	-5.70	-1260	.00889	.0308	-1245	.01956	-6.37	.00032	.00080	.0010	2.00			
173	.7901	330.65	.01	-4.31	-.0682	.01116	.0251	-.0671	.01445	-4.65	.00037	.00080	.0010	2.00			
174	.792	329.36	.01	-3.61	-.0375	.01216	.0217	-.0366	.01269	-2.88	.00013	.00080	.0010	2.00			
175	.7901	330.45	.01	-2.97	-.0163	.01289	.0192	-.0156	.01192	-1.31	.00033	.00080	.0010	2.00			
176	.7903	330.11	.01	-2.28	.0133	.01379	.0155	-.0139	.01145	1.21	.00036	.00080	.0010	2.00			
177	.773	328.91	.01	-1.63	.0367	.01441	.0129	.0371	.01156	3.21	.00036	.00080	.0010	2.00			
178	.792	329.57	.01	-.97	.0610	.01492	.0105	.0612	.01199	5.11	.00036	.00080	.0010	2.00			
179	.7901	330.52	.01	-.30	.0846	.01499	.0081	.0847	.01274	6.65	.00038	.00080	.0010	2.00			
180	.791	330.24	.01	.33	.1074	.01503	.0061	.1073	.01384	7.75	.00039	.00080	.0010	2.00			
181	.7903	330.18	.01	1.07	.1372	.01492	.0036	.1369	.01568	8.74	.00039	.00080	.0010	2.00			
182	.7903	329.70	.01	1.75	.1647	.01499	.0013	.1642	.01421	9.02	.00040	.00080	.0010	2.00			
183	.792	329.36	.01	2.41	.1932	.01528	-.0025	.1924	.02160	8.91	.00041	.00080	.0010	2.00			
184	.773	328.31	.01	3.13	.2280	.01575	-.0065	.2268	.02648	8.57	.00042	.00080	.0010	2.00			
185	.773	329.50	.00	3.89	.2660	.01566	-.0099	.2642	.03286	8.04	.00043	.00080	.0010	2.00			
186	.773	329.63	.00	4.68	.3035	.01760	-.0128	.3010	.04048	7.44	.00045	.00080	.0010	2.00			
187	.792	329.63	.00	5.45	.3404	.01871	-.0148	.3371	.04918	6.85	.00045	.00080	.0010	2.00			
188	.7903	329.84	.00	6.28	.3829	.02024	-.0164	.3784	.06022	6.28	.00050	.00080	.0010	2.00			
189	.792	329.70	.01	7.09	.4193	.02143	-.0171	.4134	.07119	5.81	.00054	.00080	.0010	2.00			
190	.792	329.56	.01	7.93	.4610	.02311	-.0178	.4534	.08468	5.35	.00056	.00080	.0010	2.00			
191	.792	329.36	.01	8.78	.5055	.02500	-.0193	.4959	.10007	4.95	.00058	.00080	.0010	2.00			
192	.7903	329.70	.01	9.56	.5473	.02715	-.0217	.5352	.11590	4.67	.00059	.00080	.0010	2.00			
193	.7903	329.56	.00	-5.72	-1268	.00890	.0310	-1253	.01970	-6.36	.00031	.00080	.0010	2.00			

SCAT 15-F

TEST 503				RUN 10		MACH 1.200									
POINT	MINF	Q	BETA	ALPHA	CN	CA	CM	CL	CD	L/D	CDC	CDB	CPI	R/FT	
217	1.202	417.64	.00	-5.53	-.1167	.01214	.0367	-.1150	.02023	-5.68	.00113	.00210	.0010	2.00	
218	1.200	417.64	.01	-4.11	-.0881	.01435	.0274	-.0569	.01538	-3.70	.00117	.00210	.0010	2.00	
219	1.201	417.51	.01	-3.39	-.0272	.01543	.0224	-.0262	.01391	-1.89	.00117	.00210	.0010	2.00	
220	1.201	417.53	.01	-2.78	-.0020	.01617	.0182	-.0012	.01316	-.09	.00117	.00210	.0010	2.00	
221	1.200	417.30	.01	-2.03	.0279	.01700	.0129	.0285	.01290	2.21	.00118	.00210	.0010	2.00	
222	1.200	417.28	.01	-1.37	.0531	.01758	.0086	.0535	.01320	4.05	.00118	.00210	.0010	2.00	
223	1.201	417.50	.01	-.65	.0824	.01806	.0037	.0826	.01403	5.89	.00118	.00210	.0010	2.00	
224	1.201	417.50	.01	.08	.1102	.01838	-.0009	.1102	.01543	7.14	.00121	.00210	.0010	2.00	
225	1.201	417.56	.01	.73	.1370	.01954	-.0051	.1368	.01719	7.66	.00124	.00210	.0010	2.00	
226	1.201	417.59	.01	1.46	.1679	.01869	-.0101	.1674	.01996	8.43	.00127	.00210	.0010	2.00	
227	1.201	417.50	.01	2.18	.2016	.01917	-.0157	.2007	.02373	8.46	.00130	.00210	.0010	2.00	
228	1.201	417.50	.00	2.92	.2408	.02005	-.0218	.2394	.02947	8.12	.00133	.00210	.0010	2.00	
229	1.203	417.42	.01	3.76	.2791	.02111	-.0270	.2771	.03626	7.64	.00133	.00210	.0010	2.00	
230	1.200	417.40	.00	4.60	.3183	.02239	-.0313	.3155	.04472	7.05	.00135	.00210	.0010	2.00	
231	1.200	417.47	.01	5.45	.3576	.02384	-.0348	.3537	.05461	6.48	.00136	.00210	.0010	2.00	
232	1.203	417.32	.01	6.29	.3956	.02535	-.0379	.3904	.06543	5.97	.00137	.00210	.0010	2.00	
233	1.203	417.36	.01	7.14	.4360	.02712	-.0409	.4293	.07801	5.50	.00139	.00210	.0010	2.00	
234	1.199	417.33	.01	8.03	.4781	.02934	-.0437	.4693	.09273	5.06	.00143	.00210	.0010	2.00	
235	1.203	417.30	.01	8.86	.523	.03009	-.0447	.5027	.10425	4.91	.00147	.00210	.0010	2.00	
736	1.209	417.31	.00	-5.53	-.1197	.01202	.0372	-.1180	.02051	-5.75	.00113	.00210	.0010	2.00	

SCAT 15-F

TEST 503			RUN 16		MACH 1.200									
POINT	MINF	Q	BETA	ALPHA	CN	CA	CM	CL	CD	L/D	CDC	CDB	CPI	R/FT
17	1.200	417.21	.00	-5.59	-.1225	.01269	.0382	-.1207	.02146	-5.62	.00112	.00210	.0010	2.00
18	1.200	417.26	.01	-4.17	-.0635	.01490	.0293	-.0623	.01638	-3.80	.00114	.00210	.0010	2.00
19	1.200	417.26	.01	-3.41	-.0312	.01598	.0241	-.0302	.01471	-2.05	.00117	.00210	.0010	2.00
20	1.200	417.26	.01	-2.73	-.0047	.01675	.0196	-.0039	.01385	-.28	.00118	.00210	.0010	2.00
21	1.200	417.26	.01	-2.04	.0236	.01744	.0147	.0242	.01348	1.80	.00119	.00210	.0010	2.00
22	1.200	417.26	.01	-1.33	.0515	.01793	.0098	.0519	.01363	3.81	.00119	.00210	.0010	2.00
23	1.201	417.29	.01	-.64	.0794	.01828	.0050	.0796	.01420	5.57	.00121	.00210	.0010	2.00
24	1.201	417.29	.01	.05	.1062	.01857	.0003	.1062	.01557	6.82	.00121	.00210	.0010	2.00
25	1.201	417.29	.01	.70	.1324	.01874	-.0041	.1322	.01726	7.66	.00125	.00210	.0010	2.00
26	1.201	417.29	.01	1.41	.1647	.01891	.0093	.1642	.01996	8.27	.00129	.00210	.0010	2.00
27	1.201	417.29	.01	2.16	.1977	.01934	-.0149	.1968	.02367	7.31	.00131	.00210	.0010	2.00
28	1.200	417.24	.00	2.92	.2349	.02013	-.0205	.2336	.02898	6.05	.00133	.00210	.0010	2.00
29	1.200	417.17	.00	3.71	.2731	.02108	-.0256	.2711	.03568	5.60	.00134	.00210	.0010	2.00
30	1.200	417.17	.00	4.57	.3131	.02223	-.0299	.3103	.04400	5.05	.00135	.00210	.0010	2.00
31	1.197	417.09	.00	5.37	.3490	.02326	-.0329	.3453	.05271	4.55	.00137	.00210	.0010	2.00
32	1.198	416.99	.00	6.26	.3904	.02453	-.0361	.3854	.06397	4.03	.00139	.00210	.0010	2.00
33	1.198	416.96	.01	7.13	.4302	.02599	-.0387	.4237	.07610	3.57	.00139	.00210	.0010	2.00
34	1.198	417.04	.01	8.04	.4731	.02797	-.0420	.4646	.09078	3.12	.00142	.00210	.0010	2.00
35	1.199	417.04	.01	8.87	.5189	.02877	-.0431	.5095	.10460	2.67	.00146	.00210	.0010	2.00
36	1.200	417.19	.01	9.63	.5656	.02992	-.0495	.5551	.11993	2.23	.00149	.00210	.0010	2.00

APPENDIX

BODY AXIS										
PRJ 827			RUN 93			MACH 2.30				
POINT	MACH	DYN PRS	BETA	ALPHA	CL	CD	CM	CDC	CCBN	CAI
1757	2.30	454.66	.02	-7.18	-.1322	.0054	.0207	.0C11	.0C09	.0008
1758	2.30	454.90	.02	-5.88	-.0943	.0072	.0168	.0C11	.0C09	.0008
1759	2.30	454.96	.02	-4.62	-.0549	.0089	.0125	.0C11	.0009	.0008
1760	2.30	454.81	.02	-3.36	-.0149	.0104	.0083	.0C10	.0010	.0008
1761	2.30	455.14	.02	-2.11	.0257	.0117	.0039	.0C10	.0010	.0008
1762	2.30	454.84	.02	-.84	.0677	.0130	-.0007	.0C11	.0010	.0008
1763	2.30	455.14	.02	.49	.1102	.0139	-.0053	.0C11	.0010	.0008
1764	2.30	455.08	.03	1.82	.1552	.0151	-.0094	.0C11	.0010	.0008
1765	2.30	454.90	.03	3.15	.1949	.0164	-.0125	.0C11	.0010	.0008
1766	2.30	454.78	.03	4.49	.2346	.0184	-.0155	.0C11	.0C1C	.0008
1767	2.30	455.34	.03	5.84	.2750	.0202	-.0179	.0C11	.0009	.0008
1768	2.30	455.11	.03	7.22	.3137	.0221	-.0199	.0C11	.0009	.0008
1769	2.30	455.14	.02	-2.10	.0262	.0117	.0039	.0C11	.0010	.0008

STABILITY AXIS										
PRJ 827			RUN 93			MACH 2.30				
POINT	MACH	L/D	BETA	ALPHA	CL	CD	CM	CDC	CCBN	CAI
1757	2.30	-8.0848	.02	-7.18	-.1300	.0214	.0207	.0C1C	.0009	.0013
1758	2.30	-5.6222	.02	-5.88	-.0927	.0165	.0168	.0C10	.0C09	.0011
1759	2.30	-4.1125	.02	-4.62	-.0537	.0131	.0125	.0C10	.0009	.0010
1760	2.30	-1.2630	.02	-3.36	-.0140	.0111	.0083	.0C10	.0010	.0009
1761	2.30	2.4552	.02	-2.11	.0263	.0107	.0039	.0C10	.0010	.0008
1762	2.30	5.6689	.02	-.84	.0680	.0120	-.0007	.0C11	.0010	.0008
1763	2.30	7.4359	.02	.49	.1100	.0148	-.0053	.0C11	.0010	.0008
1764	2.30	7.7038	.03	1.82	.1545	.0200	-.0094	.0C11	.0010	.0008
1765	2.30	7.0237	.03	3.15	.1935	.0213	-.0125	.0C11	.0010	.0008
1766	2.30	6.3470	.03	4.49	.2322	.0366	-.0155	.0C11	.0010	.0008
1767	2.30	5.6502	.03	5.84	.2712	.0480	-.0179	.0011	.0009	.0008
1768	2.30	5.0407	.03	7.22	.3080	.0611	-.0199	.0C11	.0009	.0010
1769	2.30	2.5037	.02	-2.10	.0268	.0107	.0039	.0C11	.0010	.0008

BODY AXIS										
PRJ 827			RUN 95			MACH 2.70				
POINT	MACH	DYN PRS	BETA	ALPHA	CL	CD	CM	CDC	CCBN	CAI
1784	2.70	413.65	.02	-7.25	-.1131	.0058	.0166	.0C08	.0C07	.0007
1785	2.70	413.98	.02	-6.04	-.0818	.0071	.0135	.0C08	.0C07	.0007
1786	2.70	413.49	.02	-4.80	-.0496	.0084	.0102	.0C08	.0C07	.0007
1787	2.70	413.41	.02	-3.62	-.0157	.0097	.0064	.0C08	.0C07	.0007
1788	2.70	413.67	.02	-2.43	.0181	.0109	.0029	.0C08	.0C07	.0007
1789	2.70	413.63	.02	-1.23	.0531	.0121	-.0009	.0C08	.0C07	.0007
1790	2.70	413.47	.02	.04	.0899	.0132	-.0047	.0C08	.0C07	.0007
1791	2.70	413.49	.02	1.27	.1248	.0144	-.0079	.0C08	.0C07	.0007
1792	2.70	413.78	.02	2.56	.1592	.0157	-.0106	.0C08	.0C07	.0007
1793	2.70	413.71	.02	3.81	.1925	.0173	-.0128	.0C08	.0C07	.0007
1794	2.70	413.47	.02	5.05	.2248	.0187	-.0149	.0C08	.0C07	.0007
1795	2.70	413.54	.03	6.33	.2563	.0202	-.0166	.0C09	.0C07	.0007
1796	2.70	413.65	.03	7.62	.2899	.0218	-.0181	.0C09	.0006	.0007
1797	2.70	413.58	.03	8.94	.3241	.0234	-.0194	.0C09	.0006	.0007
1798	2.70	413.71	.02	-2.42	.0190	.0109	.0027	.0C08	.0C07	.0007

STABILITY AXIS										
PRJ 827			RUN 95			MACH 2.70				
POINT	MACH	L/D	BETA	ALPHA	CL	CD	CM	CDC	CCBN	CAI
1784	2.70	-5.6944	.02	-7.25	-.1111	.0195	.0166	.0C08	.0C07	.0012
1785	2.70	-5.2340	.02	-6.04	-.0802	.0155	.0135	.0C08	.0C07	.0011
1786	2.70	-3.5475	.02	-4.80	-.0435	.0123	.0102	.0C08	.0C07	.0010
1787	2.70	-1.4034	.02	-3.62	-.0148	.0106	.0064	.0C08	.0C07	.0009
1788	2.70	1.8640	.02	-2.43	.0187	.0100	.0029	.0C08	.0C07	.0008
1789	2.70	4.9055	.02	-1.23	.0534	.0109	-.0009	.0C08	.0C07	.0008
1790	2.70	6.7699	.02	.04	.0899	.0133	-.0047	.0C08	.0C07	.0007
1791	2.70	7.2606	.02	1.27	.1244	.0171	-.0079	.0C08	.0C07	.0007
1792	2.70	6.9313	.02	2.56	.1582	.0228	-.0106	.0C08	.0C07	.0007
1793	2.70	6.3591	.02	3.81	.1907	.0300	-.0128	.0C09	.0C07	.0008
1794	2.70	5.7519	.02	5.05	.2220	.0383	-.0149	.0C09	.0C07	.0008
1795	2.70	5.2108	.03	6.33	.2522	.0481	-.0166	.0C09	.0C07	.0009
1796	2.70	4.7577	.03	7.62	.2841	.0597	-.0181	.0C09	.0C08	.0010
1797	2.70	4.3268	.03	8.94	.3161	.0731	-.0194	.0C09	.0C08	.0011
1798	2.70	1.9488	.02	-2.42	.0190	.0101	.0027	.0C08	.0C07	.0008

APPENDIX

BODY AXIS			PRJ 827	RUN 146	MACH 2.30					
POINT	MACH	DYN PRS	BETA	ALPHA	CN	CA	CM	CAC	CABM	CAT
2969	2.30	452.74	-0.0	-7.35	-0.1295	.0041	.0158	.CC10	.CC09	.0008
2970	2.30	453.21	-0.0	-6.02	-0.0813	.0062	.0129	.CC10	.CC09	.0008
2971	2.30	453.30	-0.0	-4.71	-0.0519	.0080	.0095	.CC10	.CC09	.0008
2972	2.30	453.89	-0.0	-3.44	-0.0136	.0095	.0060	.CC10	.CC10	.0008
2973	2.30	453.60	-0.0	-2.18	.0255	.0109	.0025	.CC10	.CC10	.0008
2974	2.30	453.92	-0.0	-.87	.0580	.0121	-.0015	.CC10	.CC10	.0008
2975	2.30	453.98	-0.0	.50	.1108	.0130	-.0052	.CC10	.CC10	.0008
2976	2.30	454.45	-0.0	1.87	.1556	.0145	-.0084	.CC11	.CC10	.0008
2977	2.30	454.81	-0.1	3.21	.1934	.0158	-.0106	.CC11	.CC10	.0008
2978	2.30	454.01	-0.1	4.65	.2354	.0177	-.0121	.CC11	.CC10	.0008
2979	2.30	454.54	-0.1	6.01	.2723	.0194	-.0132	.CC11	.CC09	.0008
2980	2.30	454.93	-0.2	7.43	.3119	.0213	-.0145	.CC11	.CC09	.0008
2981	2.30	454.19	-0.2	8.80	.3504	.0232	-.0159	.CC11	.CC09	.0008
2982	2.30	455.28	-0.0	-2.17	.0257	.0108	.0025	.CC10	.CC10	.0008

STABILITY AXIS			PRJ 827	RUN 146	MACH 2.30					
POINT	MACH	L/D	BETA	ALPHA	CL	CD	CM	CDC	CCBN	CDI
2969	2.30	-6.3289	-0.0	-7.35	-0.1275	.0201	.0158	.CC10	.CC09	.0013
2970	2.30	-5.8199	-0.0	-6.02	-.0598	.0154	.0129	.CC10	.CC09	.0011
2971	2.30	-4.2109	-0.0	-4.71	-.0508	.0121	.0055	.CC10	.CC09	.0010
2972	2.30	-1.2492	-0.0	-3.44	-.0127	.0102	.0060	.CC10	.CC10	.0009
2973	2.30	2.6437	-0.0	-2.18	.0263	.0099	.0025	.CC10	.CC10	.0009
2974	2.30	6.1893	-0.0	-.87	.0683	.0110	-.0015	.CC10	.CC10	.0008
2975	2.30	7.9039	-0.0	.50	.1107	.0140	-.0052	.CC10	.CC10	.0008
2976	2.30	7.9265	-0.0	1.87	.1549	.0195	-.0084	.CC11	.CC10	.0008
2977	2.30	7.2119	-0.1	3.21	.1920	.0206	-.0106	.CC11	.CC10	.0008
2978	2.30	6.3646	-0.1	4.65	.2329	.0366	-.0121	.CC11	.CC10	.0009
2979	2.30	5.8347	-0.1	6.01	.2648	.0476	-.0132	.CC11	.CC09	.0009
2980	2.30	5.0014	-0.2	7.43	.3061	.0612	-.0145	.CC11	.CC09	.0010
2981	2.30	4.4929	-0.2	8.80	.3422	.0762	-.0159	.CC11	.CC09	.0012
2982	2.30	2.6759	-0.0	-2.17	.0262	.0098	.0025	.CC10	.CC10	.0009

BODY AXIS			PRJ 827	RUN 148	MACH 2.70					
POINT	MACH	DYN PRS	BETA	ALPHA	CN	CA	CM	CAC	CABM	CAT
2999	2.70	414.29	-0.1	-7.43	-.1118	.0044	.0119	.CC08	.CC07	.0007
2999	2.70	415.27	-0.1	-6.18	-.0808	.0059	.0098	.CC08	.CC07	.0007
3001	2.70	413.87	-0.1	-4.91	-.0494	.0073	.0073	.CC08	.CC07	.0007
3002	2.70	413.76	-0.1	-3.70	-.0159	.0088	.0045	.CC08	.CC07	.0007
3003	2.70	411.89	-0.0	-2.49	.0172	.0100	.0016	.CC08	.CC07	.0007
3004	2.70	413.84	-0.0	-1.27	.0519	.0112	-.0014	.CC08	.CC07	.0007
3005	2.70	414.09	-0.0	.04	.0681	.0123	-.0046	.CC08	.CC07	.0007
3006	2.70	413.95	-0.0	1.32	.1230	.0135	-.0070	.CC08	.CC07	.0007
3007	2.70	414.15	-0.0	2.60	.1561	.0149	-.0086	.CC09	.CC07	.0007
3008	2.70	414.11	-0.0	3.86	.1886	.0163	-.0101	.CC09	.CC07	.0007
3009	2.70	413.60	-0.0	5.16	.2219	.0178	-.0113	.CC09	.CC07	.0007
3110	2.70	414.09	-0.1	6.49	.2530	.0193	-.0121	.CC09	.CC07	.0007
3111	2.70	413.67	-0.1	7.78	.2862	.0209	-.0130	.CC09	.CC06	.0007
3112	2.70	413.84	-0.1	9.11	.3184	.0225	-.0137	.CC09	.CC06	.0007
3113	2.70	413.98	-0.1	10.45	.3521	.0241	-.0144	.CC09	.CC06	.0007
3114	2.70	414.02	-0.0	11.78	.3879	.0258	-.0154	.CC09	.CC05	.0007
3116	2.70	414.19	-0.0	-2.49	.0181	.0100	.0015	.CC08	.CC07	.0007

STABILITY AXIS			PRJ 827	RUN 148	MACH 2.70					
POINT	MACH	L/D	BETA	ALPHA	CL	CD	CM	CDC	CCBN	CDI
2999	2.70	-6.0039	-0.1	-7.43	-.1099	.0183	.0119	.CC08	.CC07	.0013
2999	2.70	-5.6129	-0.1	-6.18	-.0794	.0141	.0098	.CC08	.CC07	.0011
3001	2.70	-4.2904	-0.1	-4.91	-.0483	.0113	.0073	.CC08	.CC07	.0010
3002	2.70	-1.5681	-0.1	-3.70	-.0151	.0096	.0045	.CC08	.CC07	.0009
3003	2.70	1.9427	-0.0	-2.49	.0173	.0092	.0016	.CC08	.CC07	.0008
3004	2.70	5.2283	-0.0	-1.27	.0521	.0100	-.0014	.CC08	.CC07	.0008
3005	2.70	7.1282	-0.0	.04	.0881	.0124	-.0046	.CC08	.CC07	.0007
3006	2.70	7.4959	-0.0	1.32	.1226	.0164	-.0070	.CC08	.CC07	.0007
3007	2.70	7.0789	-0.0	2.60	.1551	.0219	-.0086	.CC09	.CC07	.0007
3008	2.70	6.4557	-0.0	3.86	.1869	.0290	-.0101	.CC09	.CC07	.0008
3009	2.70	5.8232	-0.0	5.16	.2191	.0376	-.0113	.CC09	.CC06	.0008
3110	2.70	5.2347	-0.1	6.48	.2489	.0476	-.0121	.CC09	.CC06	.0009
3111	2.70	4.7349	-0.1	7.78	.2804	.0592	-.0130	.CC09	.CC06	.0010
3112	2.70	4.3029	-0.1	9.11	.3104	.0771	-.0137	.CC09	.CC06	.0012
3113	2.70	3.9262	-0.1	10.45	.3414	.0870	-.0144	.CC09	.CC06	.0014
3114	2.70	3.6062	-0.0	11.78	.3740	.1037	-.0154	.CC09	.CC05	.0016
3116	2.70	2.0418	-0.0	-2.49	.0187	.0091	.0015	.CC08	.CC07	.0008

BODY AXIS			PRJ 827	RUN 150	MACH 2.30					
POINT	MACH	DYN PRS	BETA	ALPHA	CN	CA	CM	CAC	CABM	CAT
3150	2.30	453.49	-0.0	-7.27	-.1186	.0038	.0178	.CC10	.CC09	.0.0000
3151	2.30	453.62	-0.0	-5.93	-.0990	.0053	.0153	.CC10	.CC09	.0.0000
3152	2.30	453.60	-0.0	-4.59	-.0607	.0068	.0127	.CC10	.CC09	.0.0000
3153	2.30	454.19	-0.0	-3.35	-.0239	.0081	.0097	.CC10	.CC09	.0.0000
3154	2.30	454.87	-0.0	-2.04	.0165	.0094	.0061	.CC10	.CC09	.0.0000
3155	2.30	454.95	-0.0	-.75	.0573	.0105	.0025	.CC10	.CC09	.0.0000
3156	2.30	454.07	-0.0	.67	.1026	.0114	-.0012	.CC10	.CC09	.0.0000
3157	2.30	454.31	-0.0	1.99	.1431	.0124	-.0039	.CC11	.CC09	.0.0000
3158	2.30	454.51	-0.1	3.35	.1817	.0136	-.0058	.CC11	.CC09	.0.0000
3159	2.30	454.75	-0.1	4.76	.2202	.0151	-.0066	.CC11	.CC09	.0.0000
3160	2.30	454.90	-0.1	6.20	.2588	.0166	-.0074	.CC10	.CC09	.0.0000
3161	2.30	453.95	-0.2	7.59	.2956	.0182	-.0082	.CC10	.CC09	.0.0000
3162	2.30	453.95	-0.2	8.50	.3212	.0194	-.0093	.CC10	.CC09	.0.0000
3163	2.30	454.67	-0.0	-2.04	.0162	.0093	.0061	.CC10	.CC09	.0.0000

APPENDIX

STABILITY AXIS			PRJ 827	RUN 150			MACH 2.30			
POINT	MACH	L/D	BETA	ALPHA	CL	CD	CN	CDC	CDYN	CDI
3150	2.30	-6.4213	.00	-7.27	-.1350	.0210	.0178	-.0010	0.0000	0.0000
3151	2.30	-6.3273	.00	-5.93	-.0980	.0155	.0155	.0010	0.0000	0.0000
3152	2.30	-5.1453	.00	-4.59	-.0500	.0117	.0127	.0010	0.0000	0.0000
3153	2.30	-2.4607	.00	-3.35	-.0234	.0095	.0097	.0010	0.0000	0.0000
3154	2.30	1.9203	.00	-2.04	.0168	.0088	.0061	.0010	0.0000	0.0000
3155	2.30	5.9206	.00	-.75	.0574	.0097	.0025	.0010	0.0000	0.0000
3156	2.30	8.1500	.00	.67	.1025	.0126	-.0012	.0010	0.0000	0.0000
3157	2.30	8.2145	.00	1.99	.1426	.0174	-.0039	.0011	0.0000	0.0000
3158	2.30	7.6539	.01	3.35	.1806	.0242	-.0058	.0011	0.0000	0.0000
3159	2.30	6.5470	.01	4.76	.2162	.0313	-.0066	.0011	0.0000	0.0000
3160	2.30	5.7439	.01	6.20	.2555	.0445	-.0074	.0010	0.0000	0.0000
3161	2.30	5.0865	.02	7.59	.2906	.0571	-.0080	.0010	0.0000	0.0000
3162	2.30	4.7219	.02	8.50	.3148	.0687	-.0085	.0010	0.0000	0.0000
3163	2.30	1.9018	.00	-2.09	.0166	.0087	-.0061	.0010	0.0000	0.0000

BODY AXIS			PRJ 827	RUN 152			MACH 2.70			
POINT	MACH	DYN PAS	BETA	ALPHA	CN	CA	CM	CAC	CASH	CAI
3179	2.70	414.46	-.00	-7.34	-.1178	.0040	.0140	-.0008	0.0000	0.0000
3180	2.70	413.60	-.00	-6.07	-.0865	.0052	.0122	-.0008	0.0000	0.0000
3181	2.70	415.02	-.00	-4.79	-.0547	.0064	.0101	-.0008	0.0000	0.0000
3182	2.70	414.19	-.00	-3.60	-.0235	.0076	.0079	-.0008	0.0000	0.0000
3183	2.70	414.15	-.00	-2.35	-.0097	.0086	.0052	-.0008	0.0000	0.0000
3184	2.70	414.02	.00	-1.11	.0441	.0098	.0025	-.0008	0.0000	0.0000
3185	2.70	414.13	.00	.16	.0793	.0107	-.0004	-.0008	0.0000	0.0000
3186	2.70	414.44	.00	1.45	.1138	.0118	-.0025	-.0008	0.0000	0.0000
3187	2.70	414.26	.00	2.76	.1465	.0128	-.0039	-.0008	0.0000	0.0000
3188	2.70	414.24	.00	4.04	.1787	.0140	-.0050	-.0008	0.0000	0.0000
3189	2.70	414.04	.01	5.34	.2109	.0153	-.0059	-.0008	0.0000	0.0000
3190	2.70	414.37	.01	6.65	.2406	.0165	-.0066	-.0008	0.0000	0.0000
3191	2.70	414.19	.01	7.98	.2728	.0179	-.0070	-.0008	0.0000	0.0000
3192	2.70	414.46	.01	9.29	.3041	.0192	-.0072	-.0008	0.0000	0.0000
3193	2.70	414.11	.02	10.63	.3375	.0207	-.0075	-.0009	0.0000	0.0000
3194	2.70	414.44	.01	11.18	.3521	.0213	-.0080	-.0008	0.0000	0.0000
3195	2.70	414.48	.00	-2.35	.0099	.0087	.0052	-.0008	0.0000	0.0000

STABILITY AXIS		PRJ 827		RUN 152		MACH 2.70				
POINT	MACH	L/D	BETA	ALPHA	CL	CD	CN	CDC	CDYN	CDI
3179	2.70	-6.41015	-.00	-7.34	-.1183	.0191	.0140	-.0008	0.0000	0.0000
3180	2.70	-5.4510	-.00	-6.07	-.0855	.0144	.0122	-.0008	0.0000	0.0000
3181	2.70	-4.9123	-.00	-4.79	-.0539	.0110	.0101	-.0008	0.0000	0.0000
3182	2.70	-2.5462	-.00	-3.60	-.0230	.0090	.0079	-.0008	0.0000	0.0000
3183	2.70	1.2203	-.00	-2.35	.0100	.0082	.0052	-.0008	0.0000	0.0000
3184	2.70	4.9636	.00	-1.11	.0442	.0089	.0025	-.0008	0.0000	0.0000
3185	2.70	7.2371	.00	.16	.0793	.0110	-.0024	-.0008	0.0000	0.0000
3186	2.70	7.7521	.00	1.45	.1134	.0146	-.0025	-.0008	0.0000	0.0000
3187	2.70	7.3351	.00	2.76	.1458	.0199	-.0039	-.0008	0.0000	0.0000
3188	2.70	6.8625	.00	4.04	.1773	.0266	-.0050	-.0008	0.0000	0.0000
3189	2.70	5.8790	.01	5.34	.2086	.0349	-.0059	-.0008	0.0000	0.0000
3190	2.70	5.1569	.01	6.65	.2370	.0442	-.0066	-.0008	0.0000	0.0000
3191	2.70	4.8173	.01	7.98	.2677	.0556	-.0070	-.0008	0.0000	0.0000
3192	2.70	4.3821	.01	9.29	.2970	.0681	-.0072	-.0008	0.0000	0.0000
3193	2.70	3.9703	.02	10.63	.3279	.0826	-.0075	-.0008	0.0000	0.0000
3194	2.70	3.8285	.01	11.18	.3413	.0891	-.0080	-.0009	0.0000	0.0000
3195	2.70	1.2455	.00	-2.35	.0103	.0083	.0052	-.0008	0.0000	0.0000

APPENDIX

SYMBOLS

ALPHA	angle of attack, deg
BETA	angle of sideslip, deg
CA	axial-force coefficient, $\frac{\text{Axial force}}{qS}$
CAB and CABN	base axial-force coefficient
CAC	chamber axial-force coefficient
CAI	internal-flow axial-force coefficient
CD	drag coefficient, $\frac{\text{Drag}}{qS}$
CDB and CABN	base-drag coefficient
CDC	chamber-drag coefficient
CDI	internal-flow drag coefficient
CM	pitching-moment coefficient, $\frac{\text{Pitching moment}}{qS\bar{c}}$
CN	normal-force coefficient, $\frac{\text{Normal force}}{qS}$
DYN PRS and Q	free-stream dynamic pressure, lb/ft ² (1 lb/ft ² = 47.88 Pa)
L/D	lift-drag ratio
MINF	free-stream Mach number
R/FT	Reynolds number per foot (1 R/FT = 0.3048 R/M)
Model component designations:	
B	fuselage
E	engine nacelles
H	horizontal tail
V	center-line-mounted and wing-mounted vertical tails

APPENDIX

W65,tip

wing with $\Lambda = 65^\circ$ at tip

W60,tip

modified wing with $\Lambda = 60^\circ$ at tip

APPENDIX

TABLE AI.- GEOMETRIC CHARACTERISTICS OF MODEL

Wing, W:

Aspect ratio	1.63
Span, cm (in.)	57.973 (22.824)
Area, m ² (ft ²)	0.207 (2.227)
Root chord at fuselage center line, cm (in.)	81.473 (32.076)
Tip chord, cm (in.)	3.429 (1.350)
Mean geometric chord, cm (in.)	48.654 (19.155)
Thickness-chord ratio, near root	0.030
Thickness-chord ratio, tip	0.027

Fuselage, B:

Length, cm (in.)	137.160 (54.000)
Balance-chamber area, m ² (ft ²)	0.0015 (0.0158)

Horizontal tail, H:

Aspect ratio, exposed	2.42
Span, exposed, cm (in.)	7.544 (2.970)
Area, exposed, m ² (ft ²)	0.0047 (0.0504)
Root chord at fuselage juncture, cm (in.)	10.201 (4.016)
Tip chord, cm (in.)	2.258 (0.889)
Mean geometric chord, cm (in.)	7.061 (2.780)
Airfoil section	Half circular arc
Thickness-chord ratio	0.030

Center-line vertical tail:

Area, m ² (ft ²)	0.0055 (0.059)
Airfoil section	Half circular arc
Thickness-chord ratio	0.025

Outboard vertical tails:

Area (each), m ² (ft ²)	0.0055 (0.059)
Airfoil section	Half circular arc
Thickness-chord ratio	0.025

Center-line ventral fin:

Area, m ² (ft ²)	0.0022 (0.024)
Airfoil section	Wedge slab

Nacelles, E:

Length, cm (in.)	17.089 (6.728)
Base area, (each), m ² (ft ²)	0.00031 (0.00336)

REFERENCES

1. Carlson, Harry W.; and Harris, Roy V., Jr.: A Unified System of Supersonic Aerodynamic Analysis. Analytic Methods in Aircraft Aerodynamics, NASA SP-228, 1970, pp. 639-658.
2. Craidon, Charlotte B.: Description of a Digital Computer Program for Airplane Configuration Plots. NASA TM X-2074, 1970.
3. Sommer, Simon C.; and Short, Barbara J.: Free-Flight Measurements of Turbulent-Boundary-Layer Skin Friction in the Presence of Severe Aerodynamic Heating at Mach Numbers From 2.8 to 7.0. NACA TN 3391, 1955.
4. Hoerner, Sigward F.: Fluid-Dynamic Drag. Hoerner Fluid Dynamics (Brick Town, N.J.), c.1965.
5. Harris, Roy V., Jr.: An Analysis and Correlation of Aircraft Wave Drag. NASA TM X-947, 1964.
6. Mack, Robert J.: A Numerical Method for Evaluation and Utilization of Supersonic Nacelle-Wing Interference. NASA TN D-5057, 1969.
7. Whitham, G. B.: The Flow Pattern of a Supersonic Projectile. Commun. Pure & Appl. Math., vol. V, no. 3, Aug. 1952, pp. 301-348.
8. Carlson, Harry W.; and Miller, David S.: Numerical Methods for the Design and Analysis of Wings at Supersonic Speeds. NASA TN D-7713, 1974.
9. Miranda, Luis R.; Elliott, Robert D.; and Baker, William M.: A Generalized Vortex Lattice Method for Subsonic and Supersonic Flow Applications. NASA CR-2865, 1977.
10. Middleton, W. D.; and Lundry, J. L.: A Computational System for Aerodynamic Design and Analysis of Supersonic Aircraft. Part 1 - General Description and Theoretical Development. NASA CR-2715, 1976.
11. Middleton, W. D.; Lundry, J. L.; and Coleman, R. G.: A Computational System for Aerodynamic Design and Analysis of Supersonic Aircraft. Part 2 - User's Manual. NASA CR-2716, 1976.
12. Middleton, W. D.; Lundry, J. L.; and Coleman, R. G.: A Computational System for Aerodynamic Design and Analysis of Supersonic Aircraft. Part 3 - Computer Program Description. NASA CR-2717, 1976.
13. Stallings, Robert L., Jr.; and Lamb, Milton: Effects of Roughness Size on the Position of Boundary-Layer Transition and on the Aerodynamic Characteristics of a 55° Swept Delta Wing at Supersonic Speeds. NASA TP-1027, 1977.

14. Decker, John P.; and Jacobs, Peter F.: Stability and Performance Characteristics of a Fixed Arrow Wing Supersonic Transport Configuration (SCAT 15F-9898) at Mach Numbers From 0.60 to 1.20. NASA TM-78726, 1978.
15. Morris, Odell A.; Fuller, Dennis E.; and Watson, Carolyn B.: Aerodynamic Characteristics of a Fixed Arrow-Wing Supersonic Cruise Aircraft at Mach Numbers of 2.30, 2.70, and 2.95. NASA TM-78706, 1978.

TABLE I.- EXTRAPOLATION OF SCAT 15-F-9898

MODEL DATA TO FULL SCALE

	Drag increment
Skin friction (model $C_{D,f} = 0.00765$; airplane $C_{d,f} = 0.00379$)	-0.00386
Roughness drag	0.00023
Wave drag (model $C_{D,w} = 0.00110$; airplane $C_{d,w} = 0.00122$)	0.00012
Grit drag	<u>-0.00040</u>
Total	-0.00391

TABLE II.- COMPONENT WETTED AREAS AND CONFIGURATION

SKIN-FRICTION COEFFICIENTS

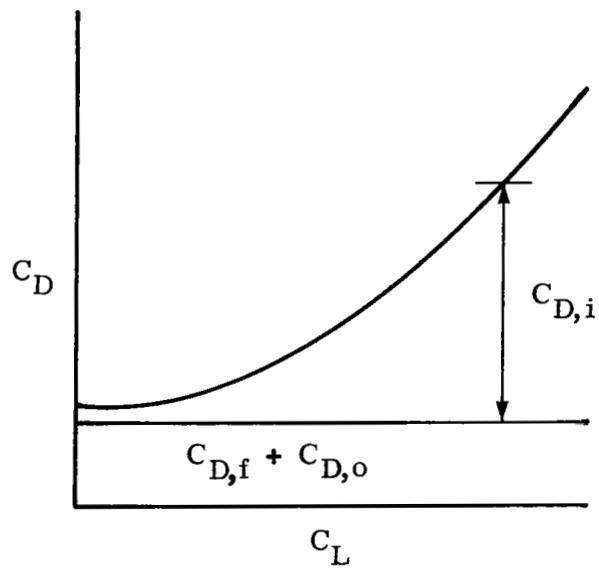
$$[S = 781.78 \text{ m}^2 (8415 \text{ ft}^2)]$$

Component	Wetted area	
	m ²	ft ²
Wing	1414.72	15 227.88
Fuselage	734.06	7901.34
Nacelles (4)	250.44	2695.70
Wing fins (2)	73.58	791.98
Vertical tail	73.96	796.11
Horizontal tail	93.30	1004.30
Total	2640.05	28 417.31

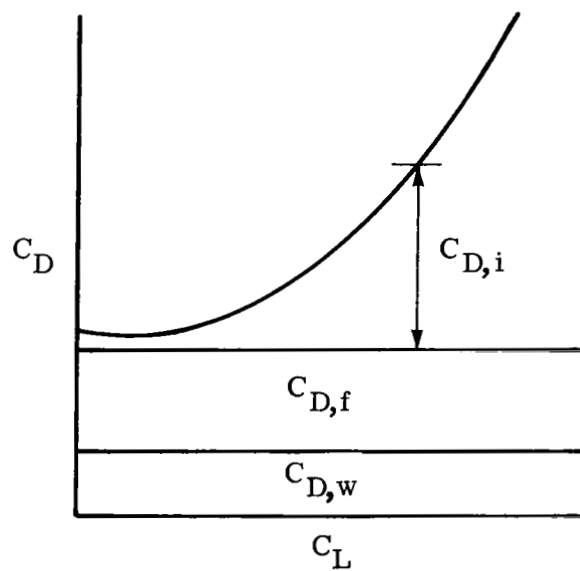
Mach number	Altitude		C _{D,f}
	m	ft	
1.20	10 375	34 040	0.005480
2.00	14 704	48 240	.004750
2.62	17 953	58 900	.004270

TABLE III.- HORIZONTAL-TAIL INCIDENCE
 ANGLES REQUIRED FOR MAXIMUM
 CONFIGURATION PERFORMANCE

M	i_t , deg
1.10	5
1.20	4
1.30	4
1.40	4
1.50	5
1.60	5
1.80	5
2.00	4
2.20	4
2.40	5
2.62	4

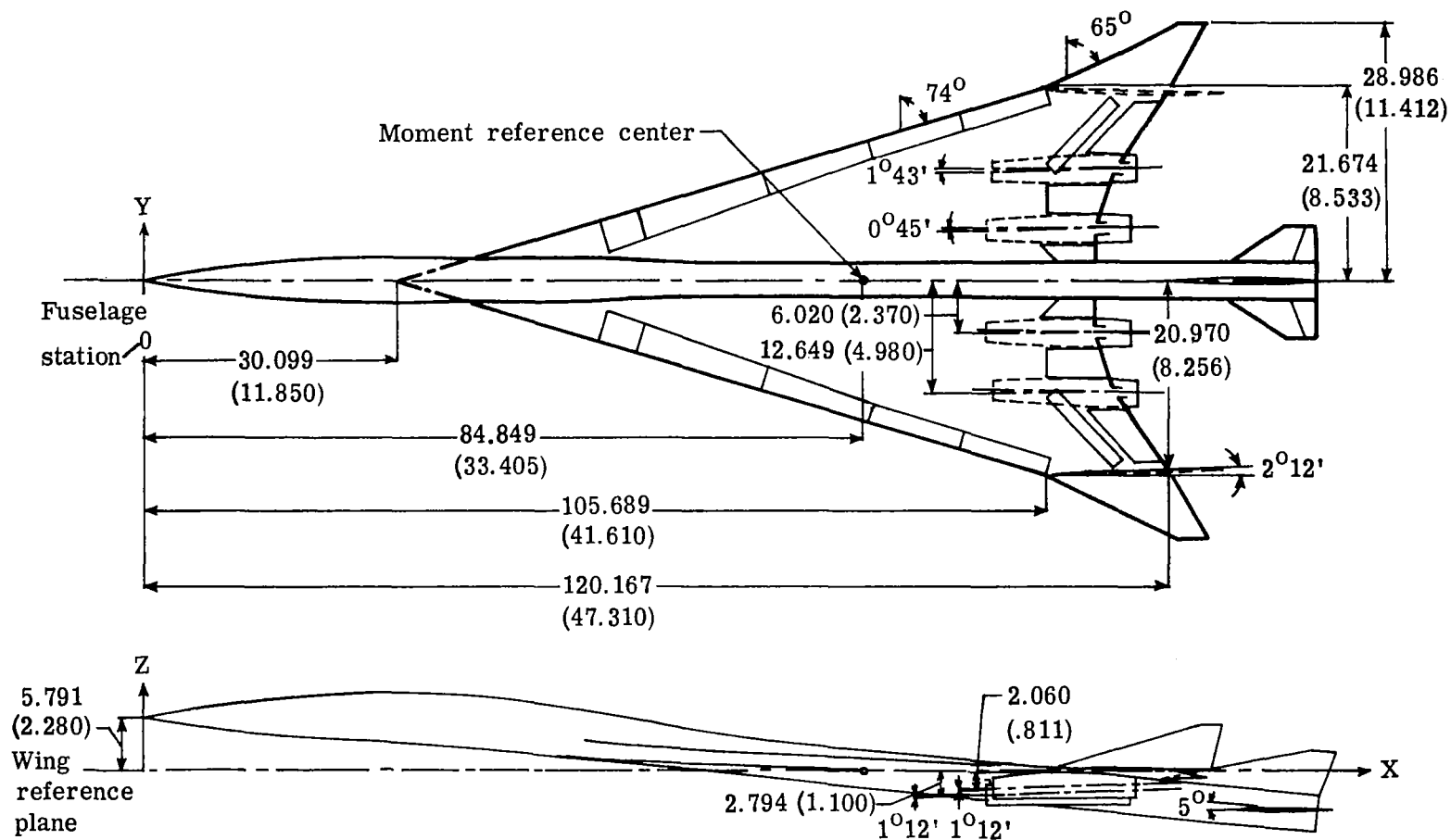


(a) Subsonic.



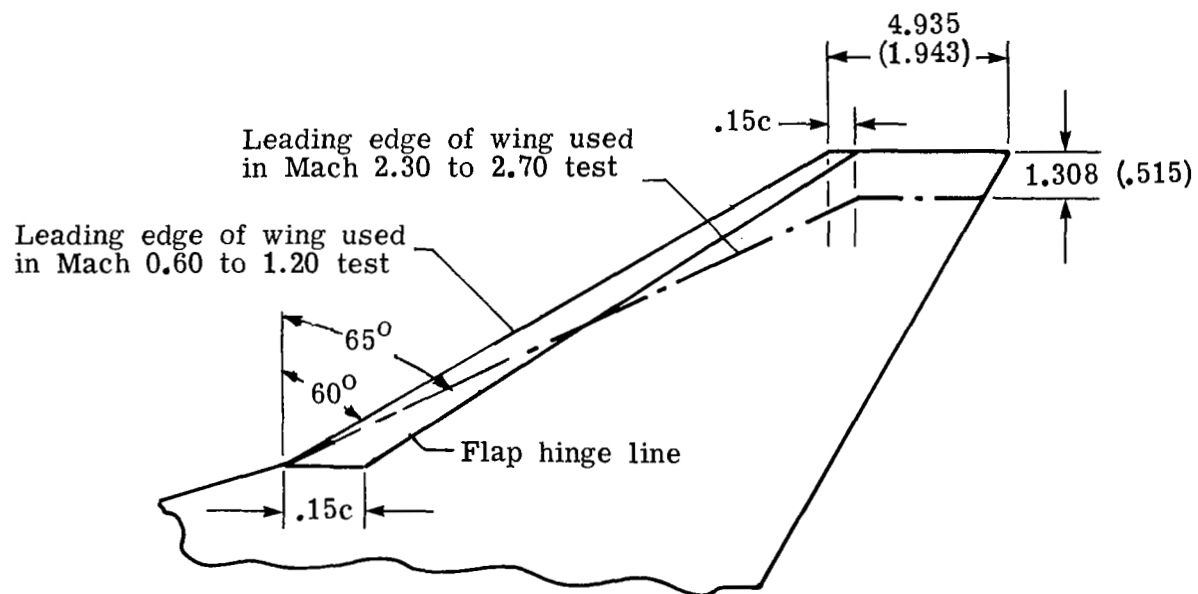
(b) Supersonic.

Figure 1.- Drag buildup procedure.



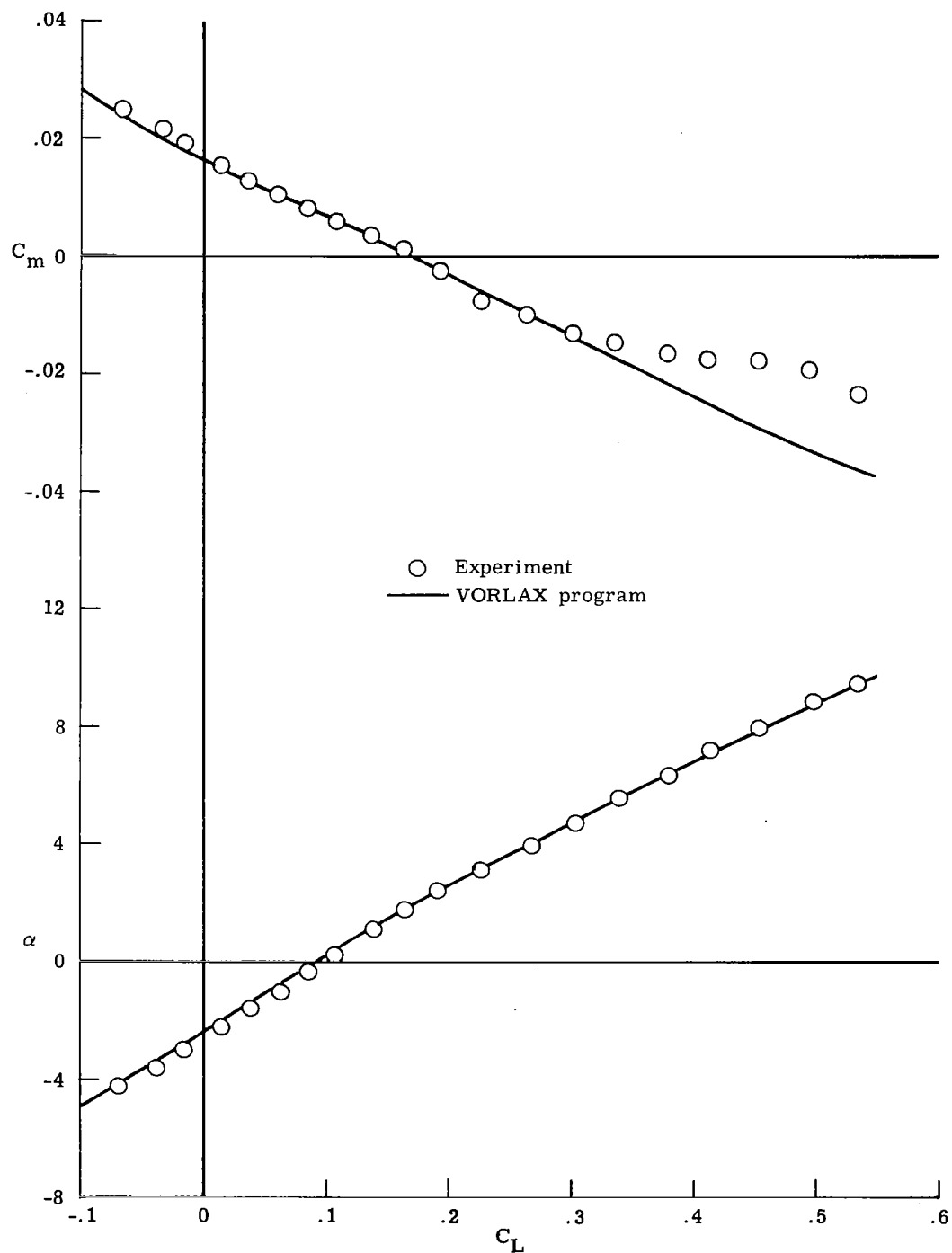
(a) Basic configuration.

Figure 2.- Details of model. Dimensions are in cm (in.) unless otherwise noted.



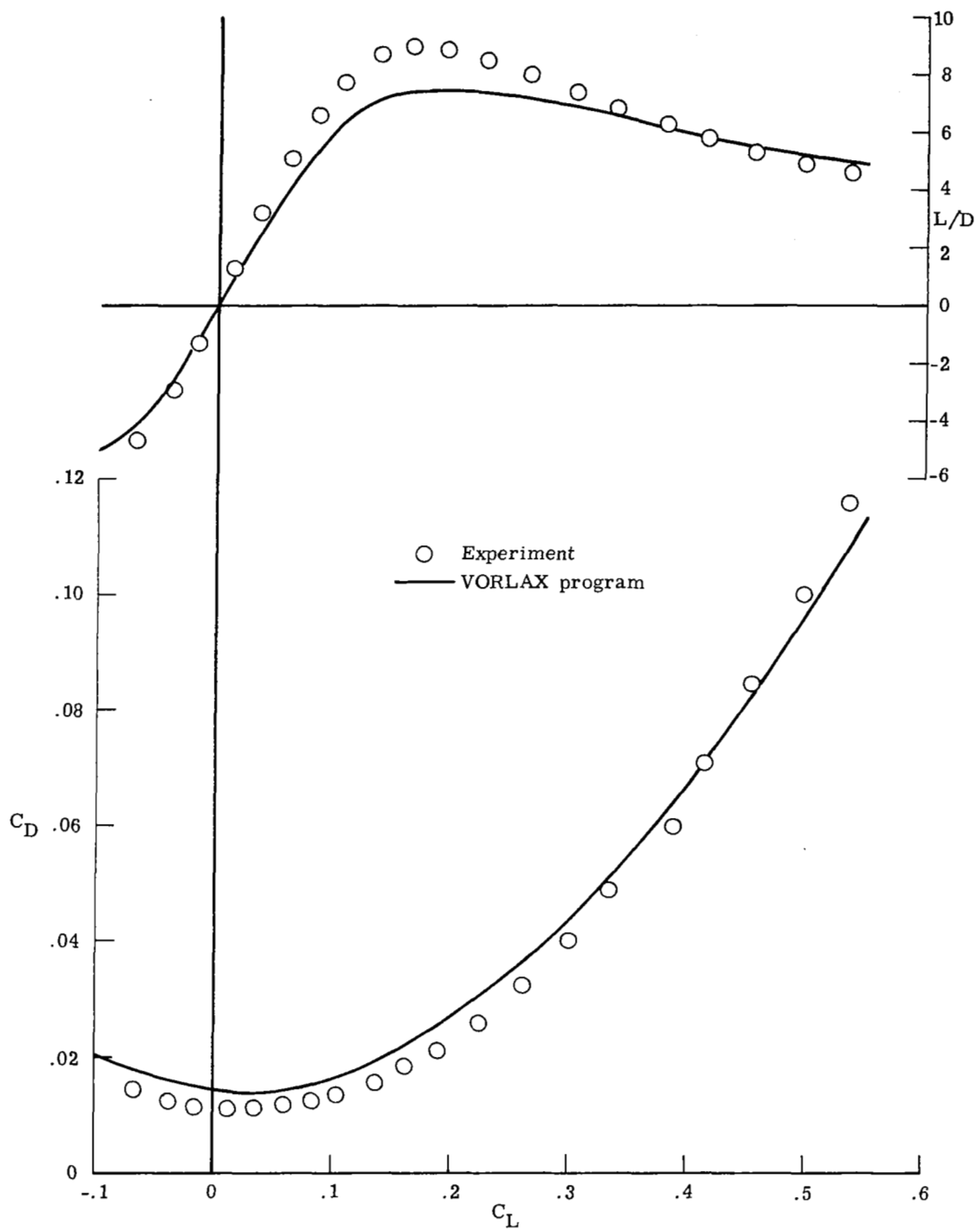
(b) Alternate wing outer panel geometry.

Figure 2.- Concluded.



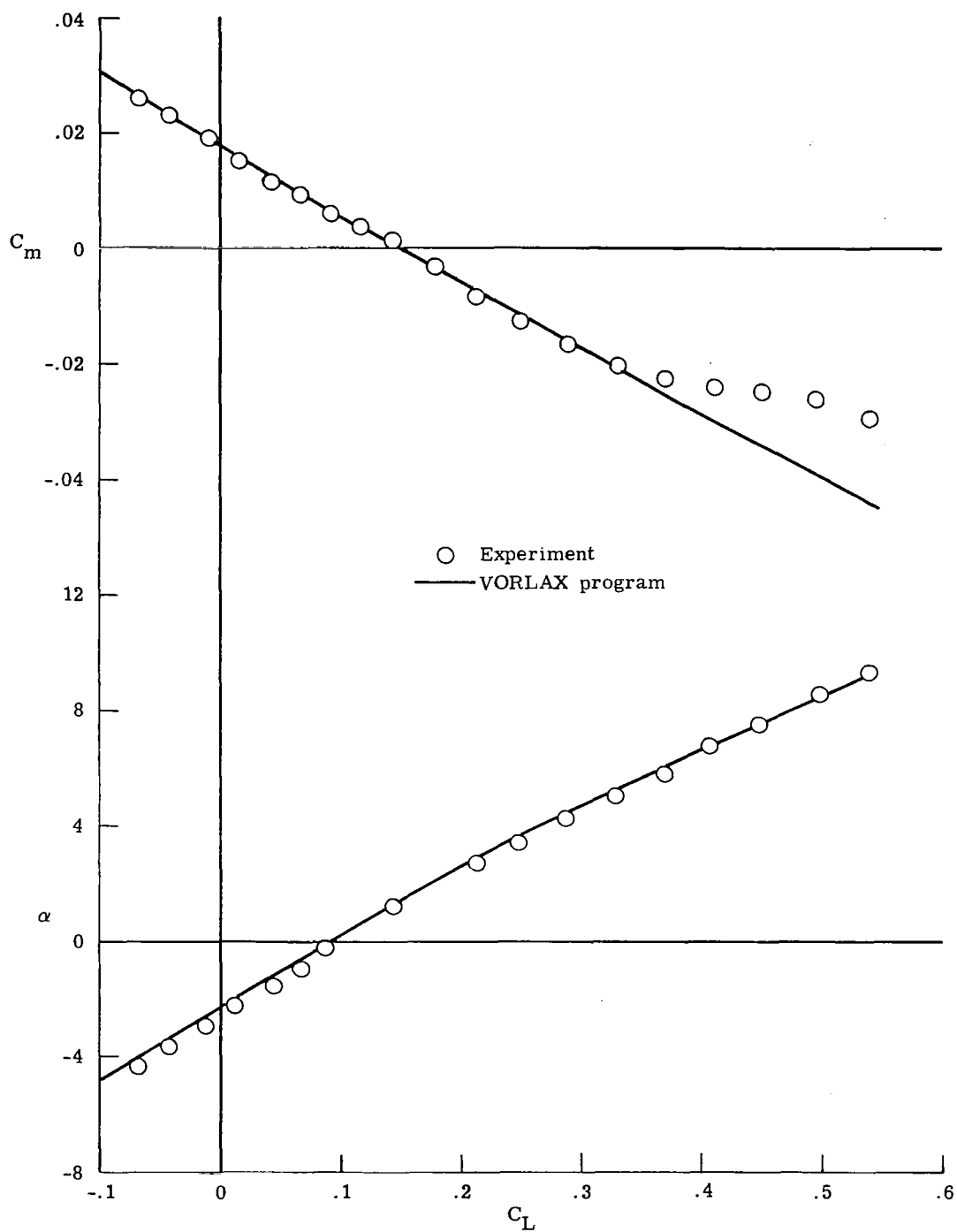
(a) $M = 0.80$.

Figure 3.- Comparison of theoretical and experimental results for complete model at subsonic speeds.



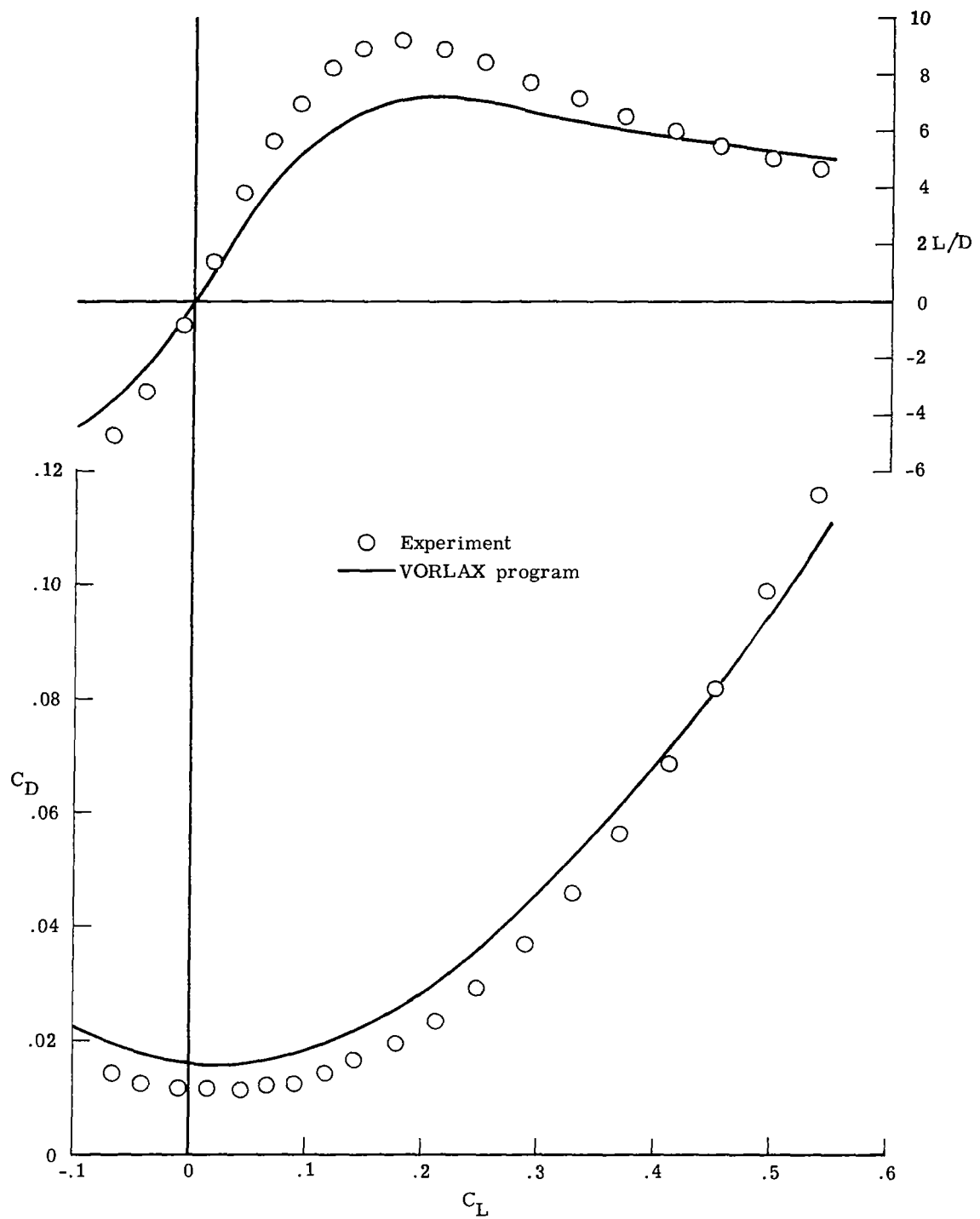
(a) Concluded.

Figure 3.- Continued.



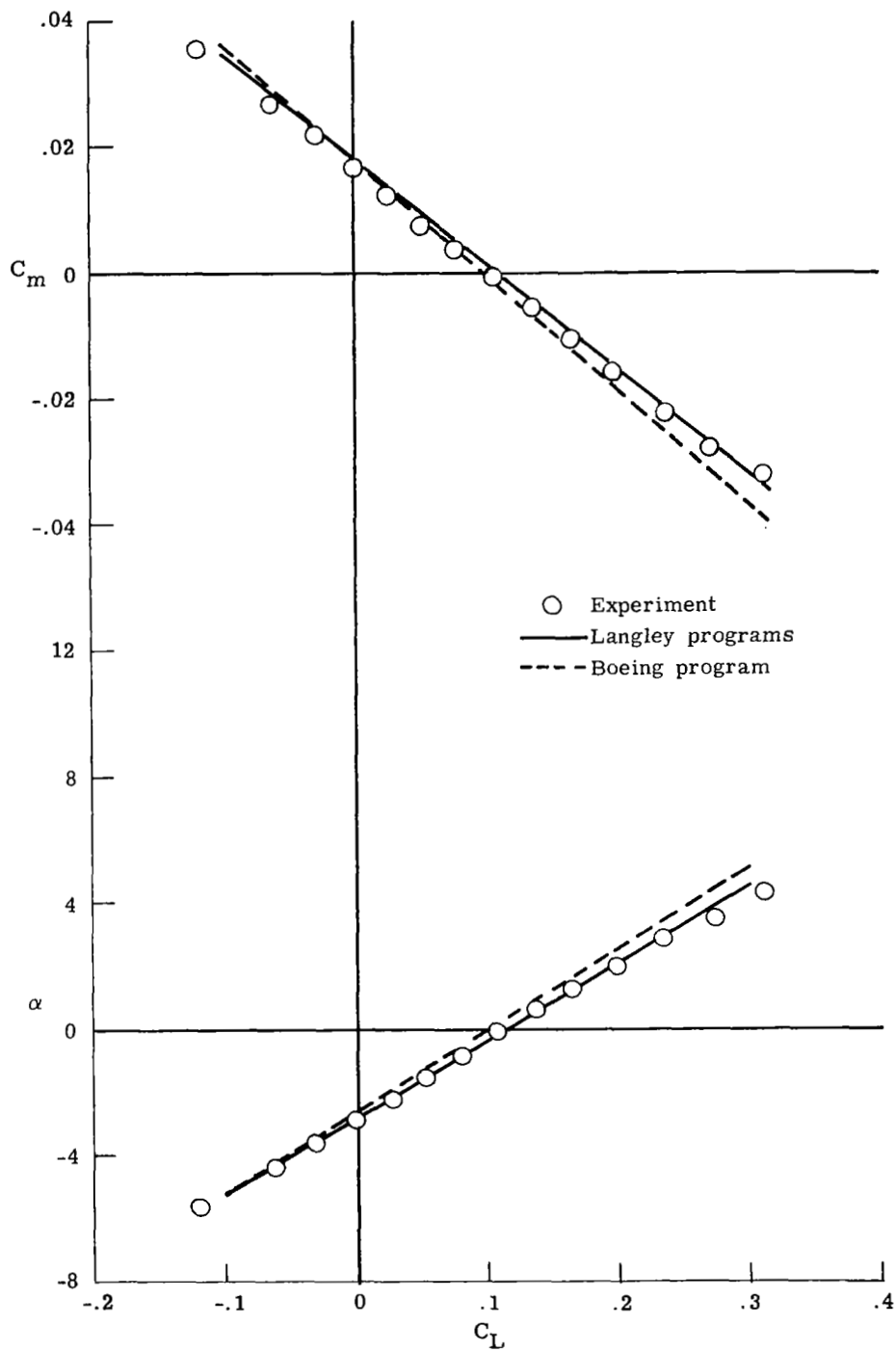
(b) $M = 0.90$.

Figure 3.- Continued.



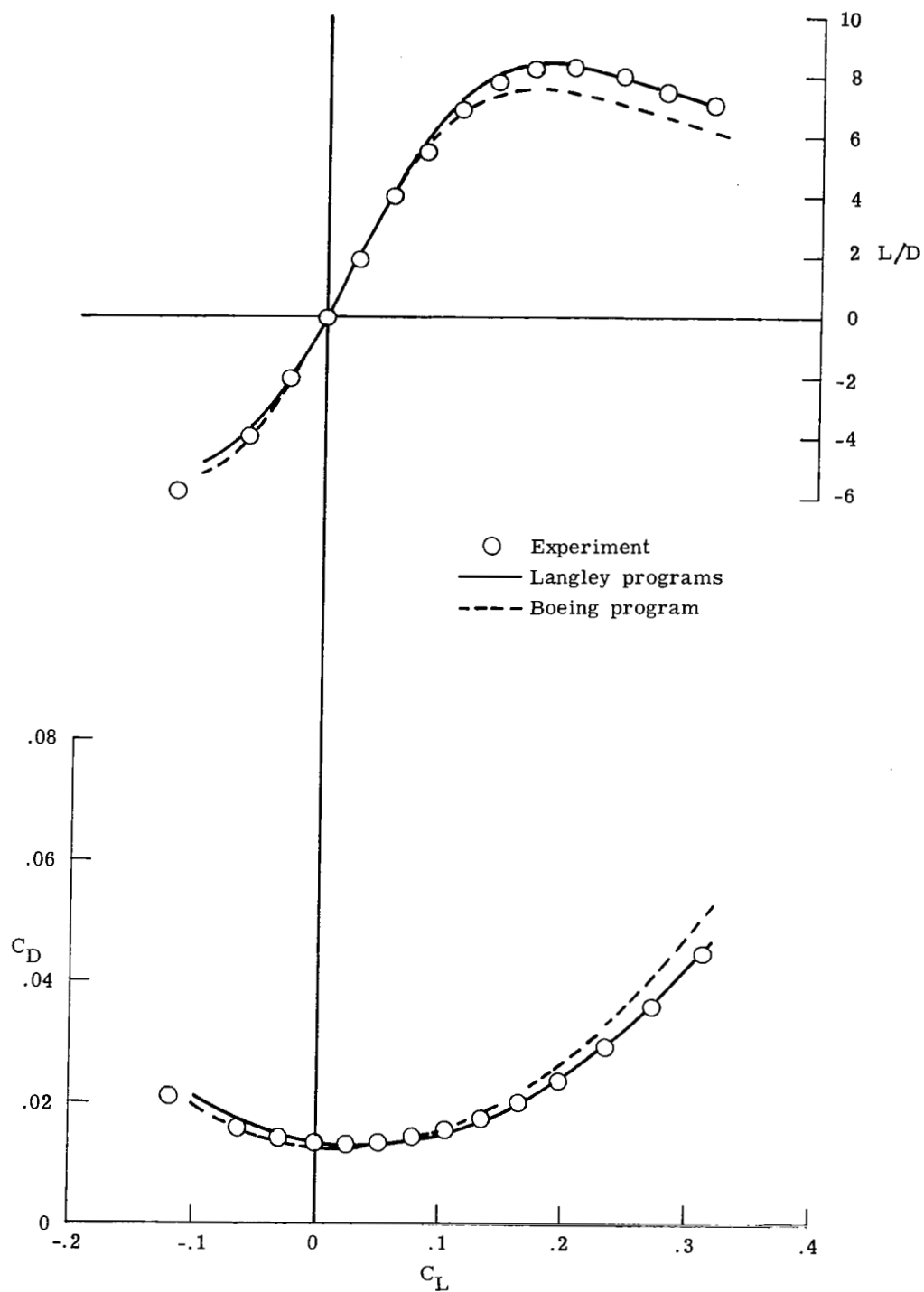
(b) Concluded.

Figure 3.- Concluded.



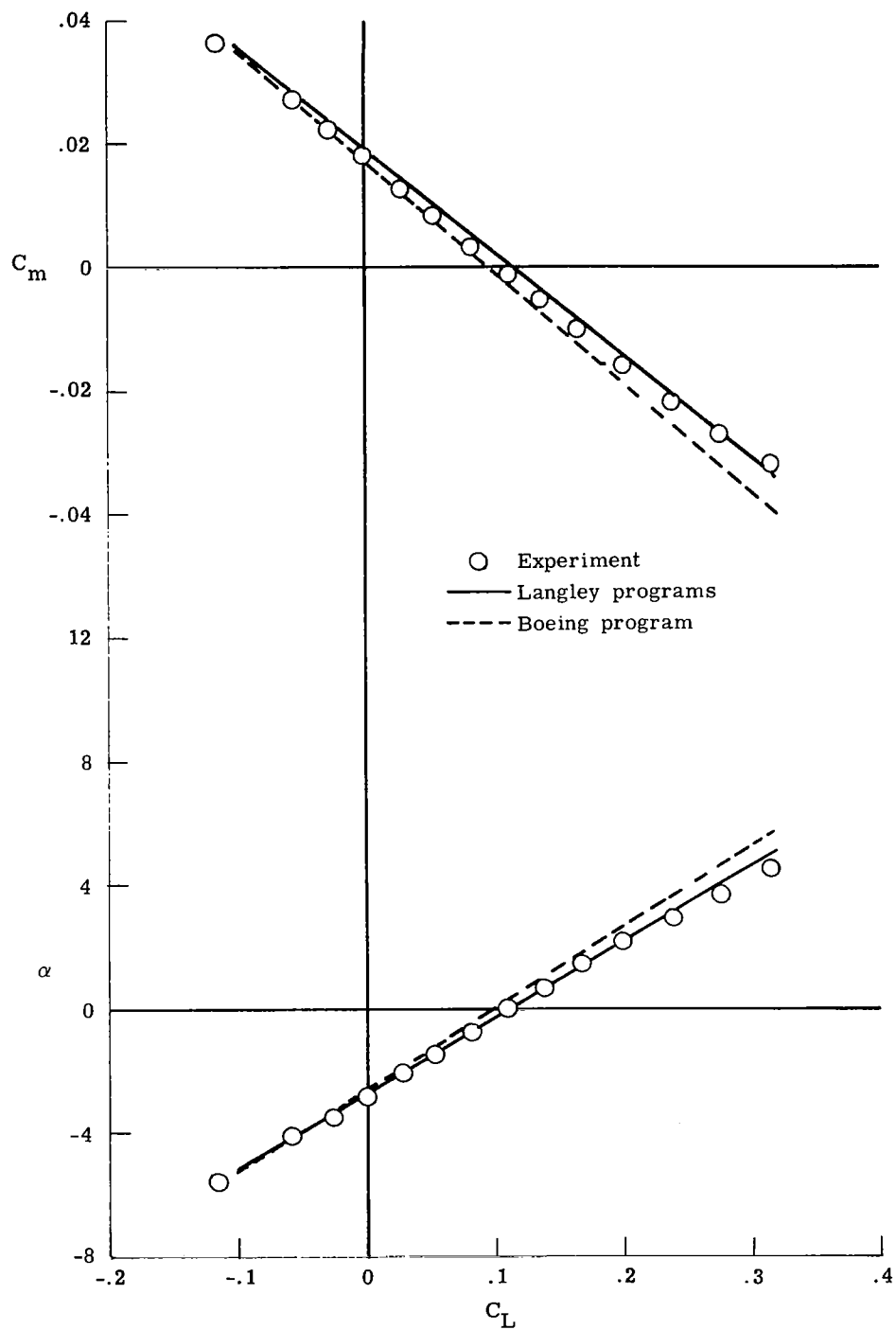
(a) $\delta_{L,6} = 0^\circ$.

Figure 4.- Comparison of theoretical and experimental results for complete model at Mach 1.20.



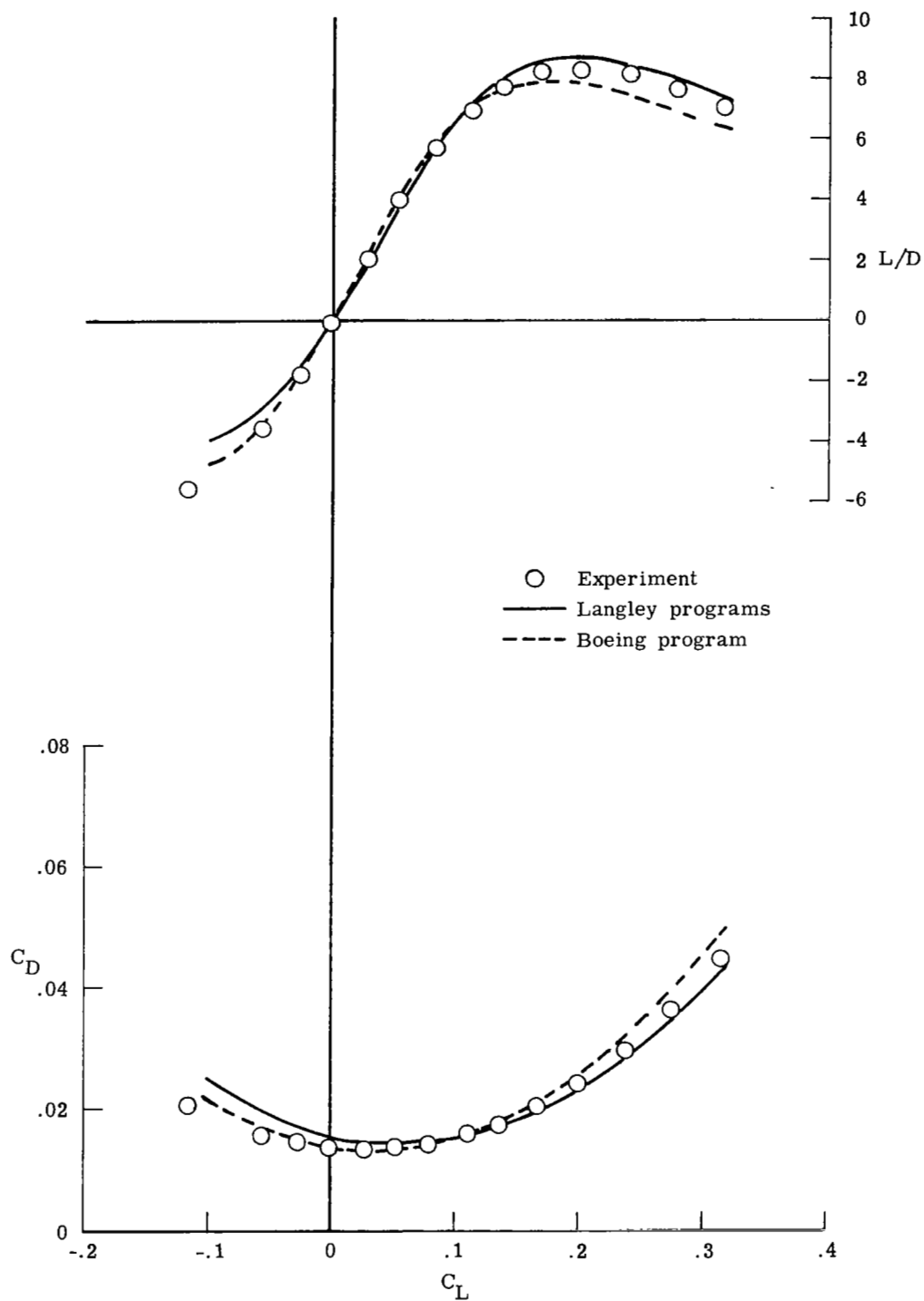
(a) Concluded.

Figure 4.- Continued.



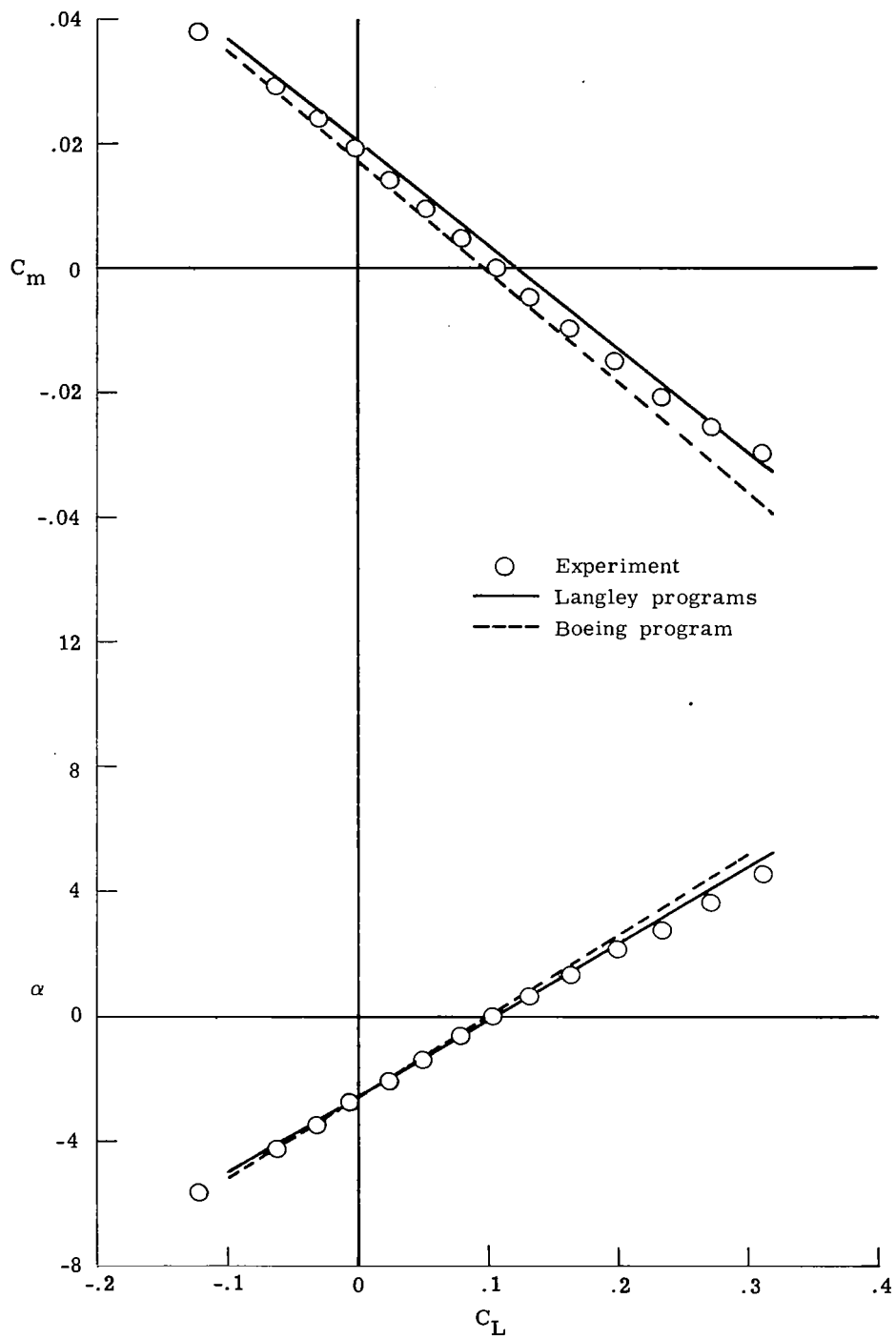
(b) $\delta_{L,6} = 10^\circ$.

Figure 4.- Continued.



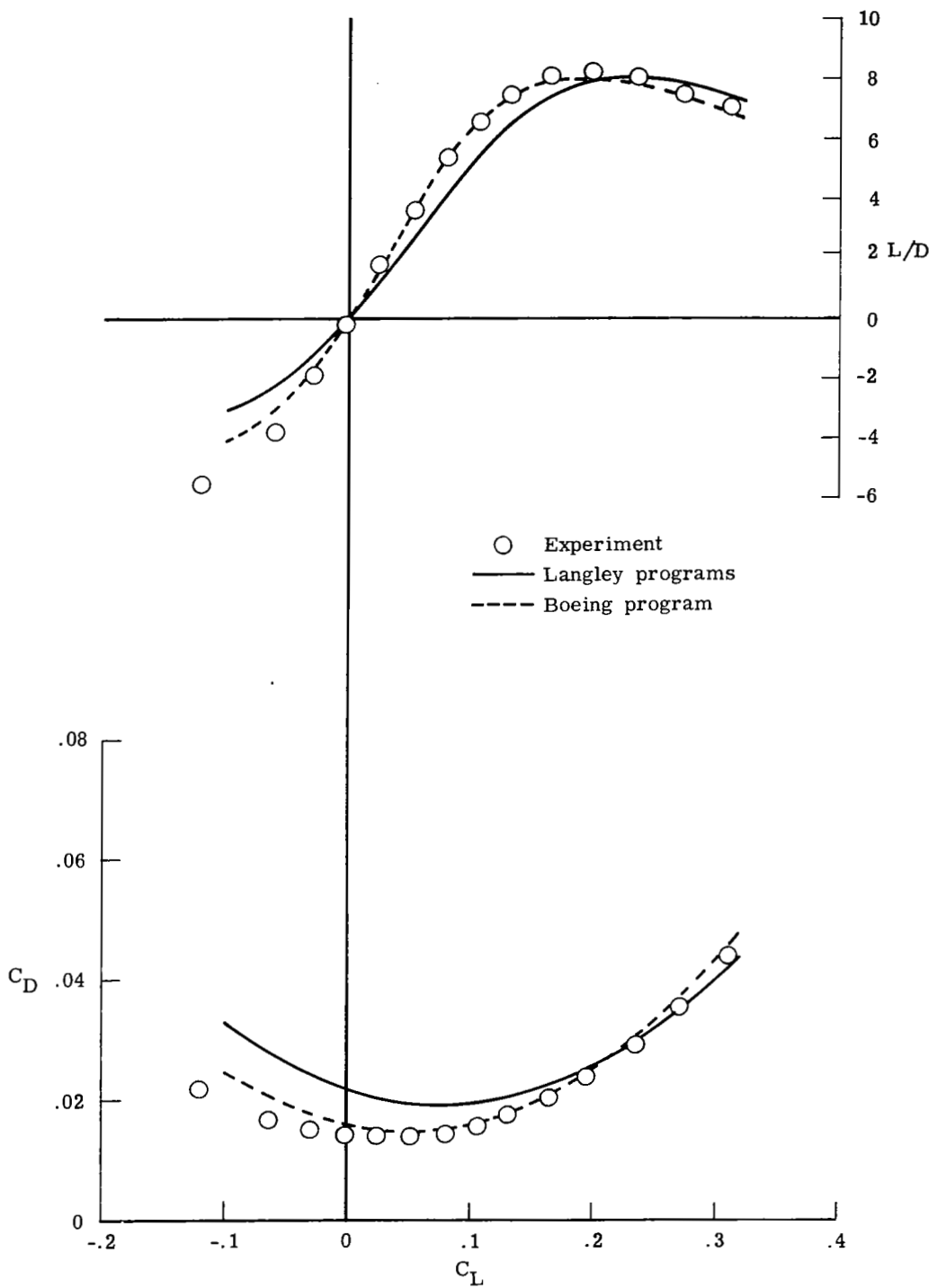
(b) Concluded.

Figure 4.- Continued.



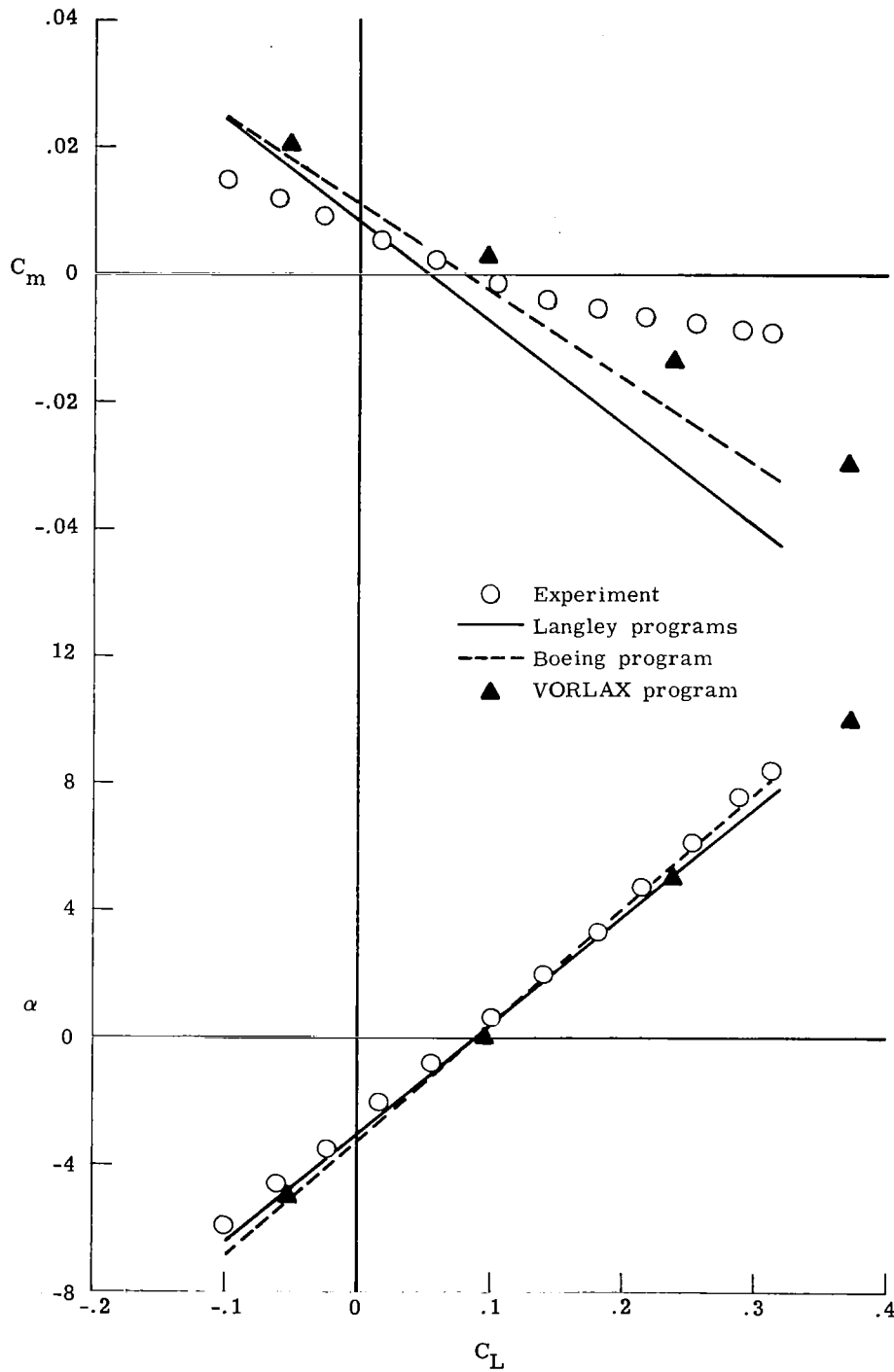
(c) $\delta_{L,6} = 20^\circ$.

Figure 4.- Continued.



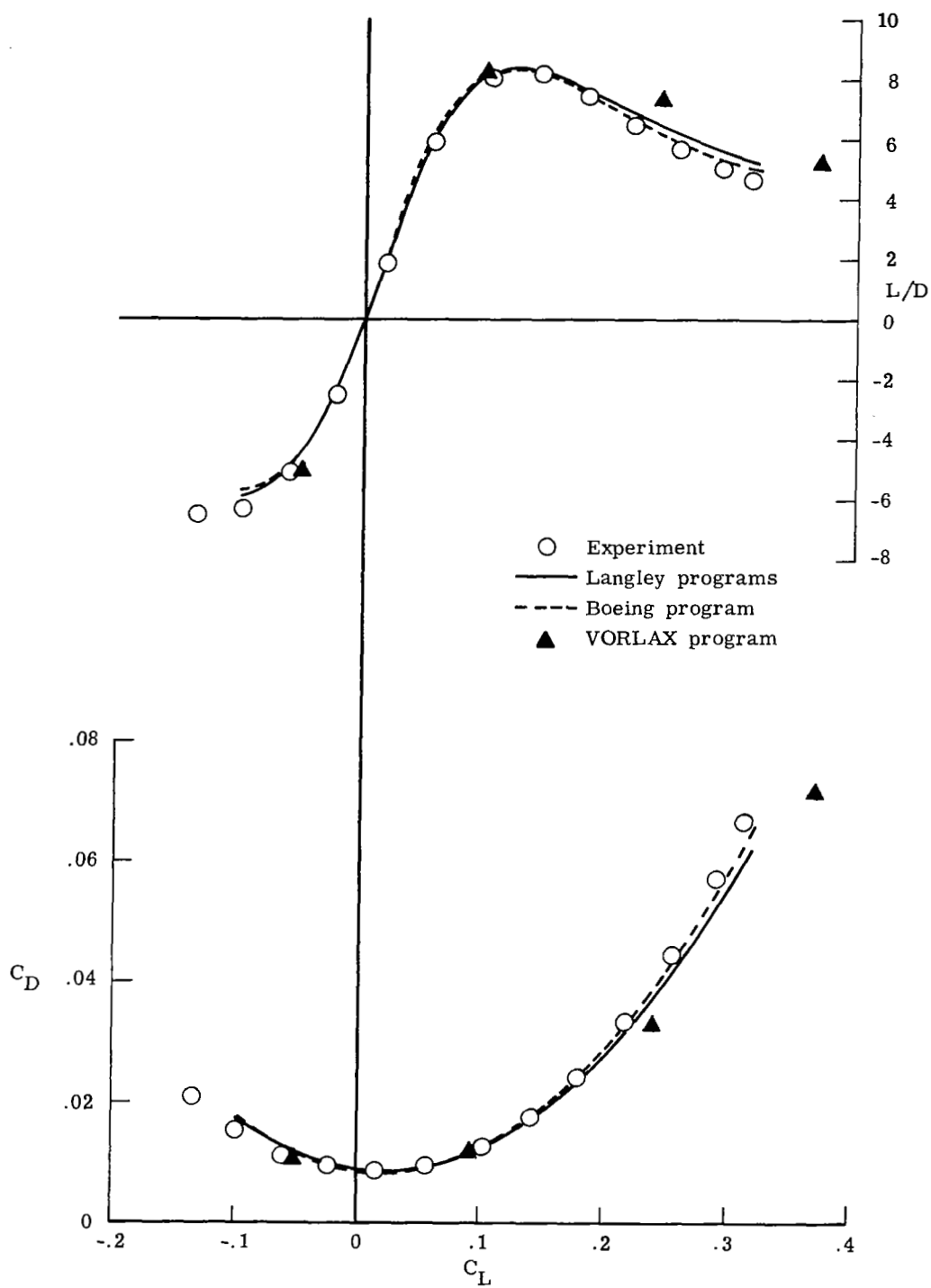
(c) Concluded.

Figure 4.- Concluded.



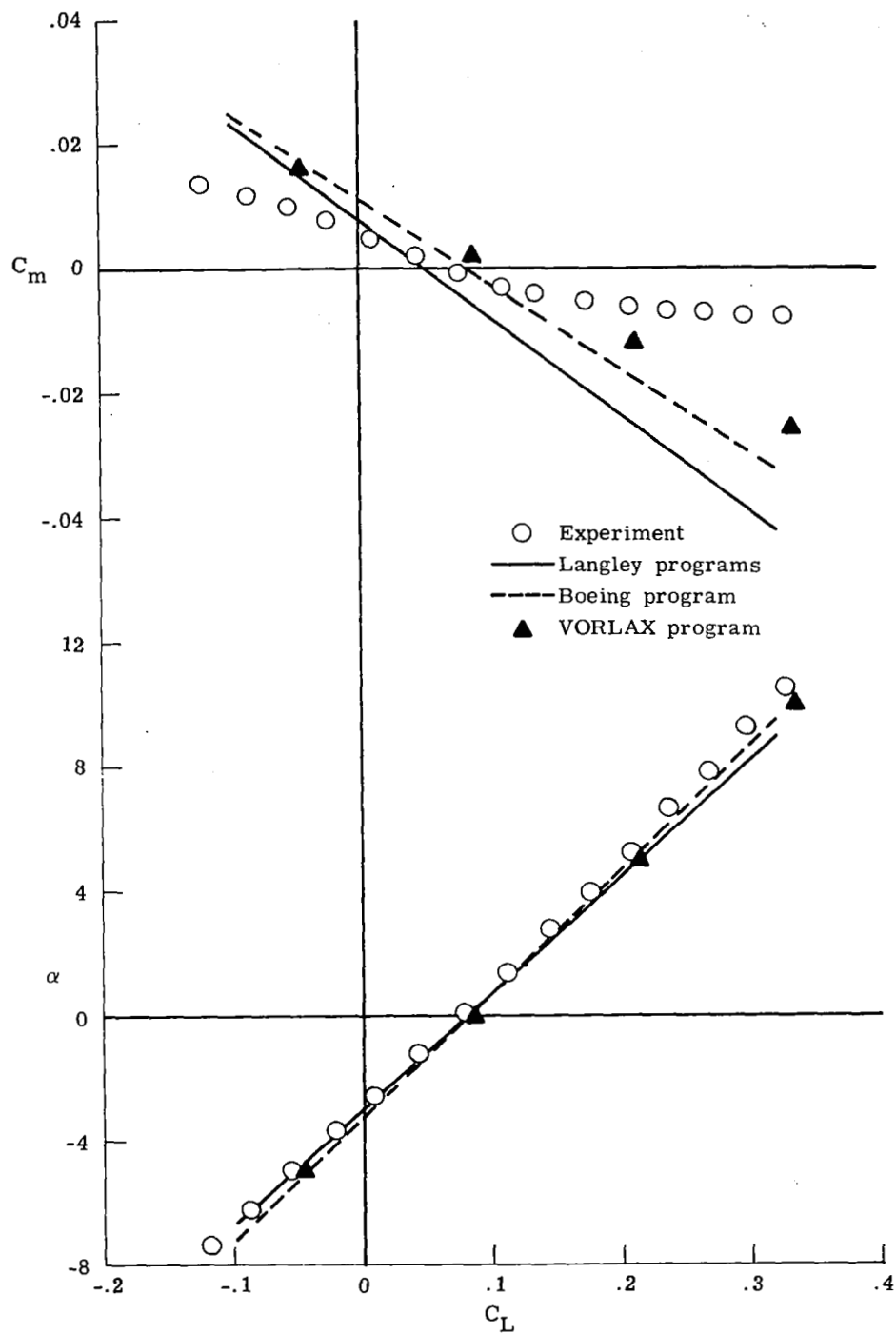
(a) $M = 2.30$.

Figure 5.- Comparison of theoretical and experimental results for wing-body at supersonic speeds.



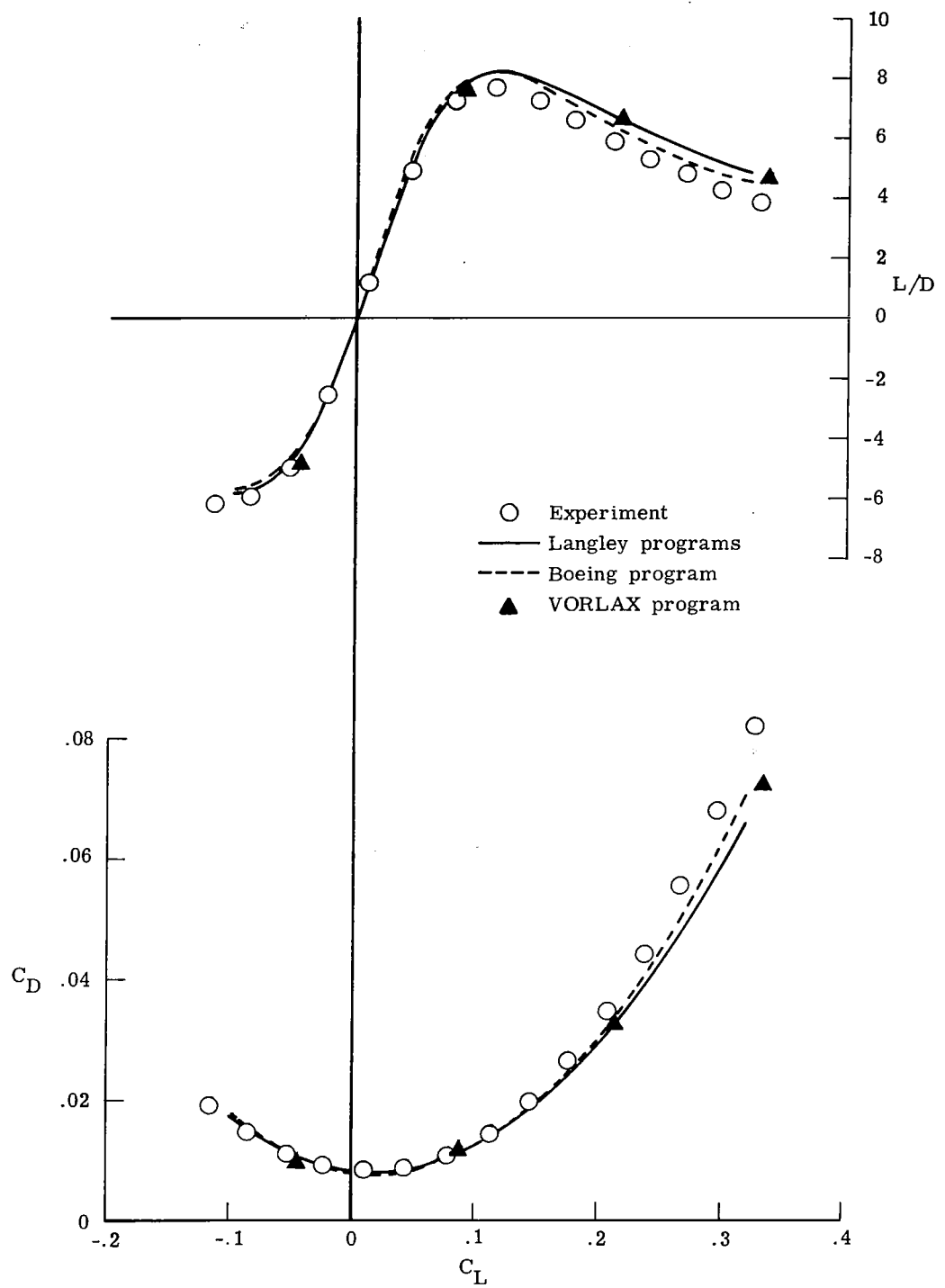
(a) Concluded.

Figure 5.- Continued.



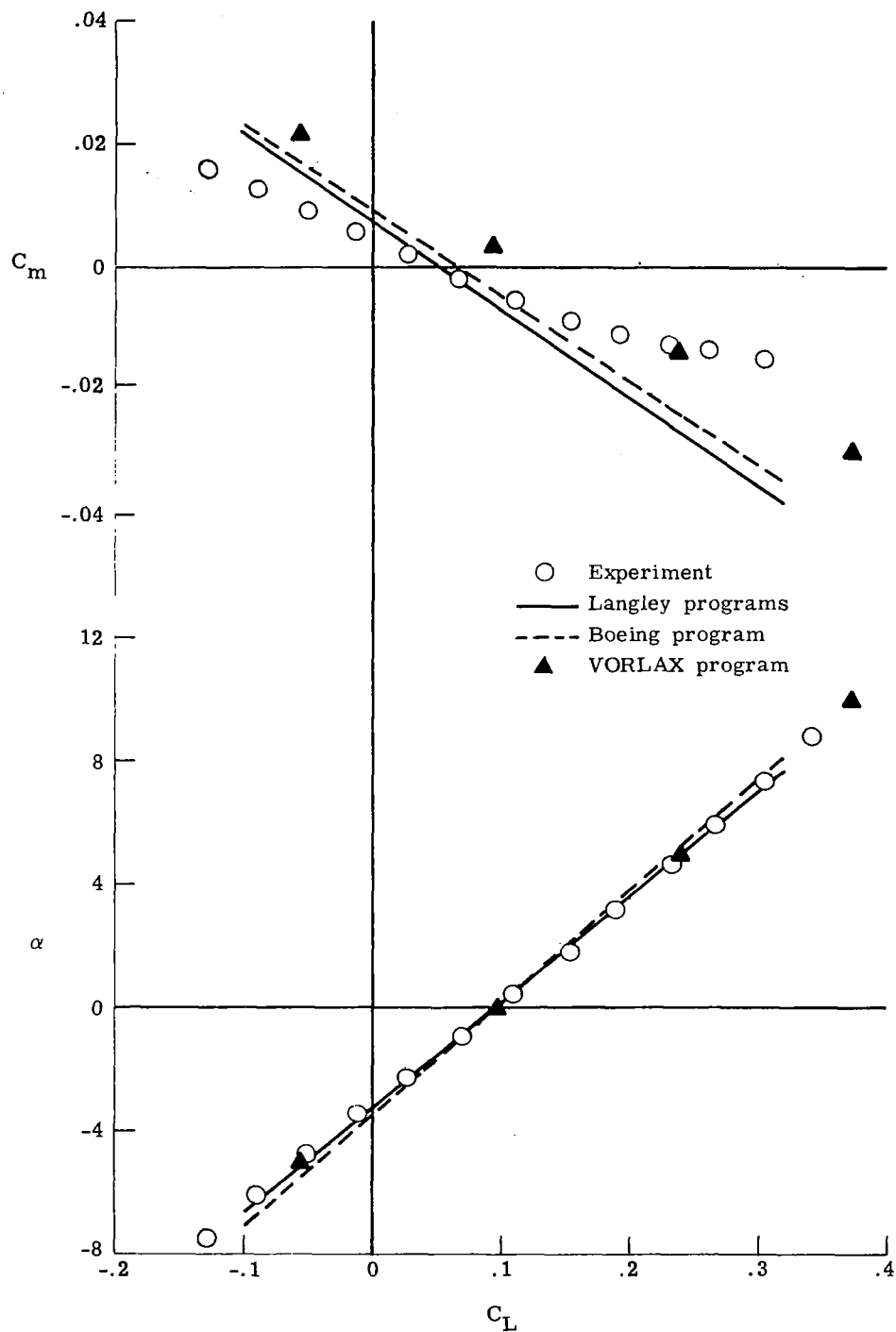
(b) $M = 2.70$.

Figure 5.- Continued.



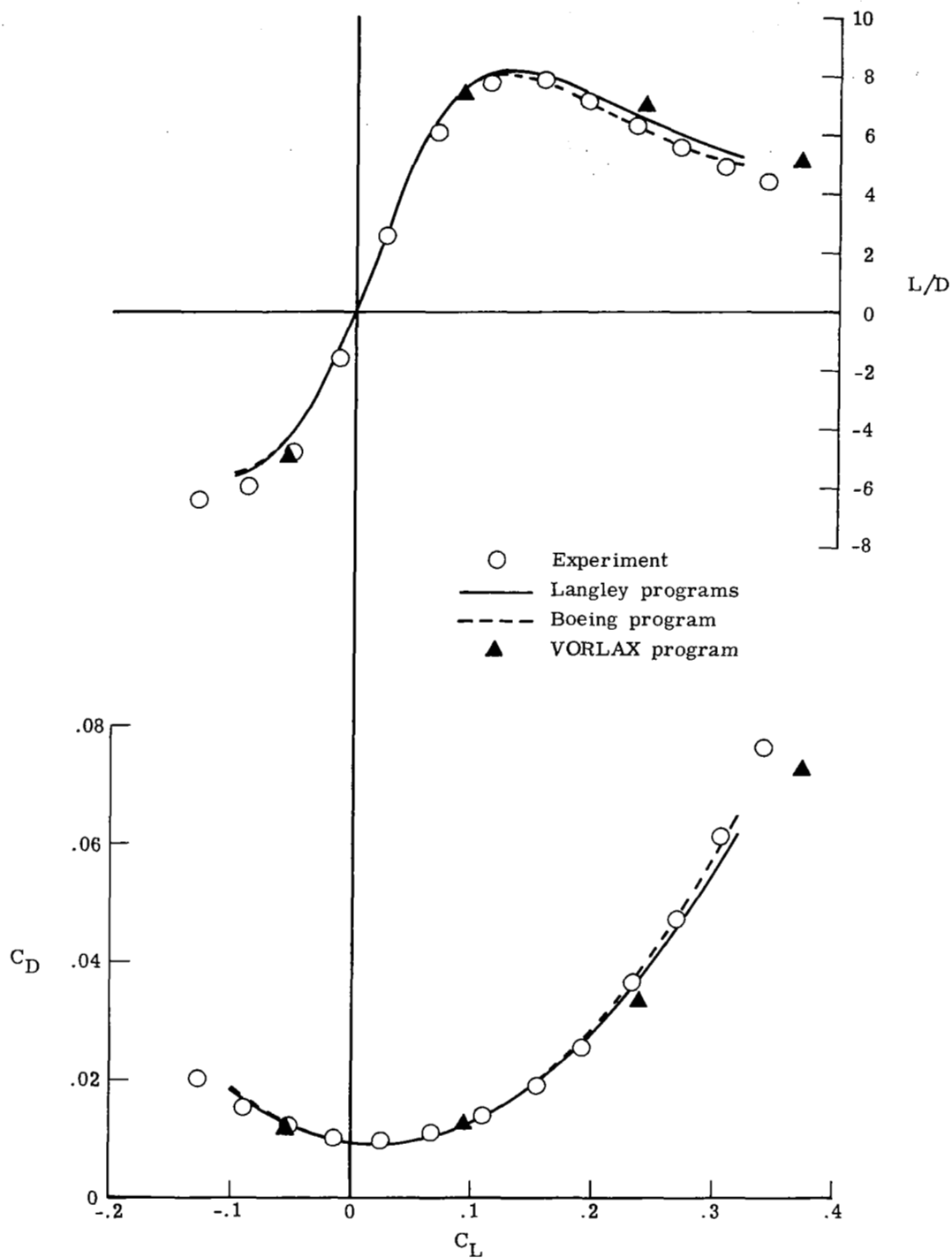
(b) Concluded.

Figure 5.- Concluded.



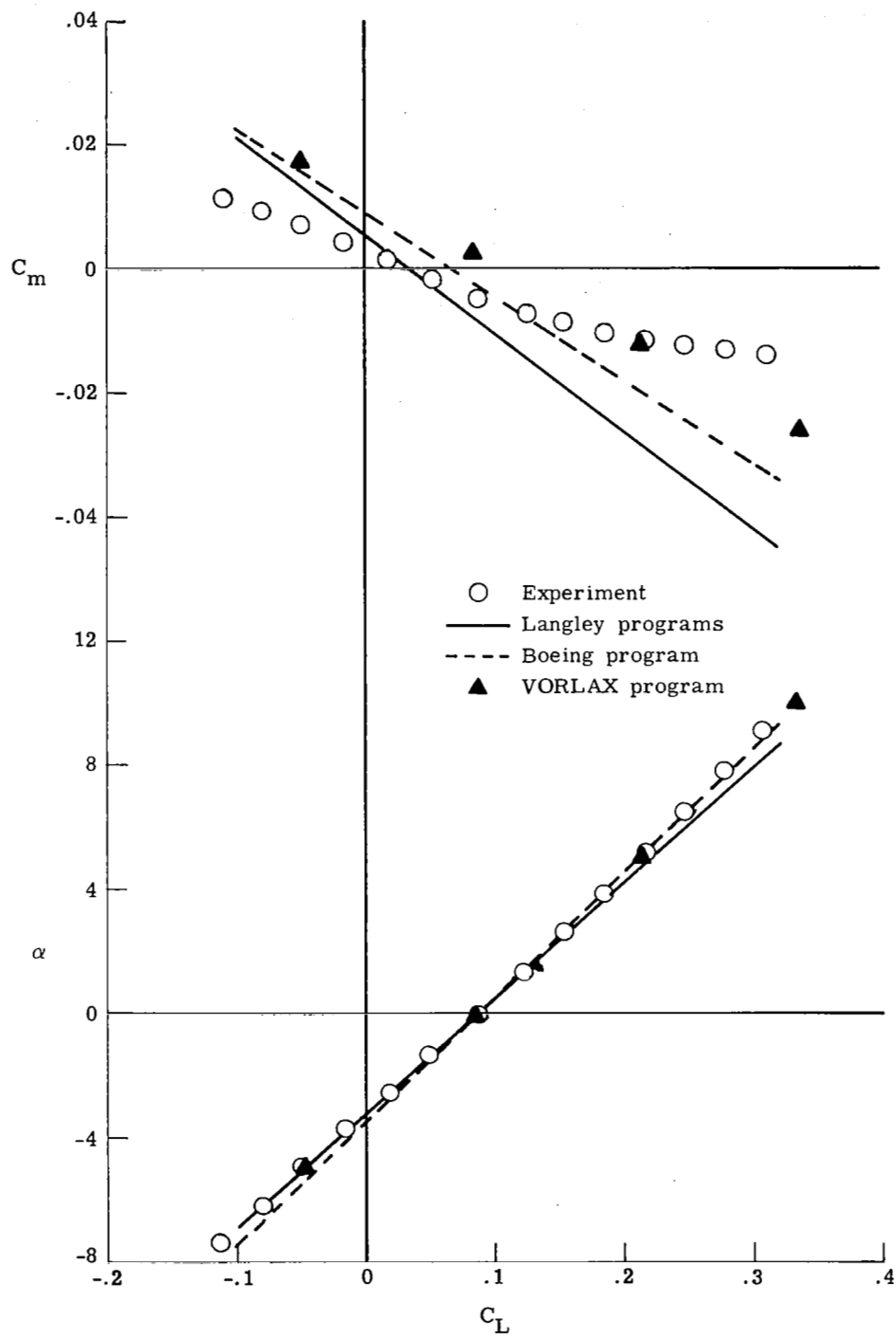
(a) $M = 2.30$.

Figure 6.- Comparison of theoretical and experimental results for wing-body-nacelles at supersonic speeds.



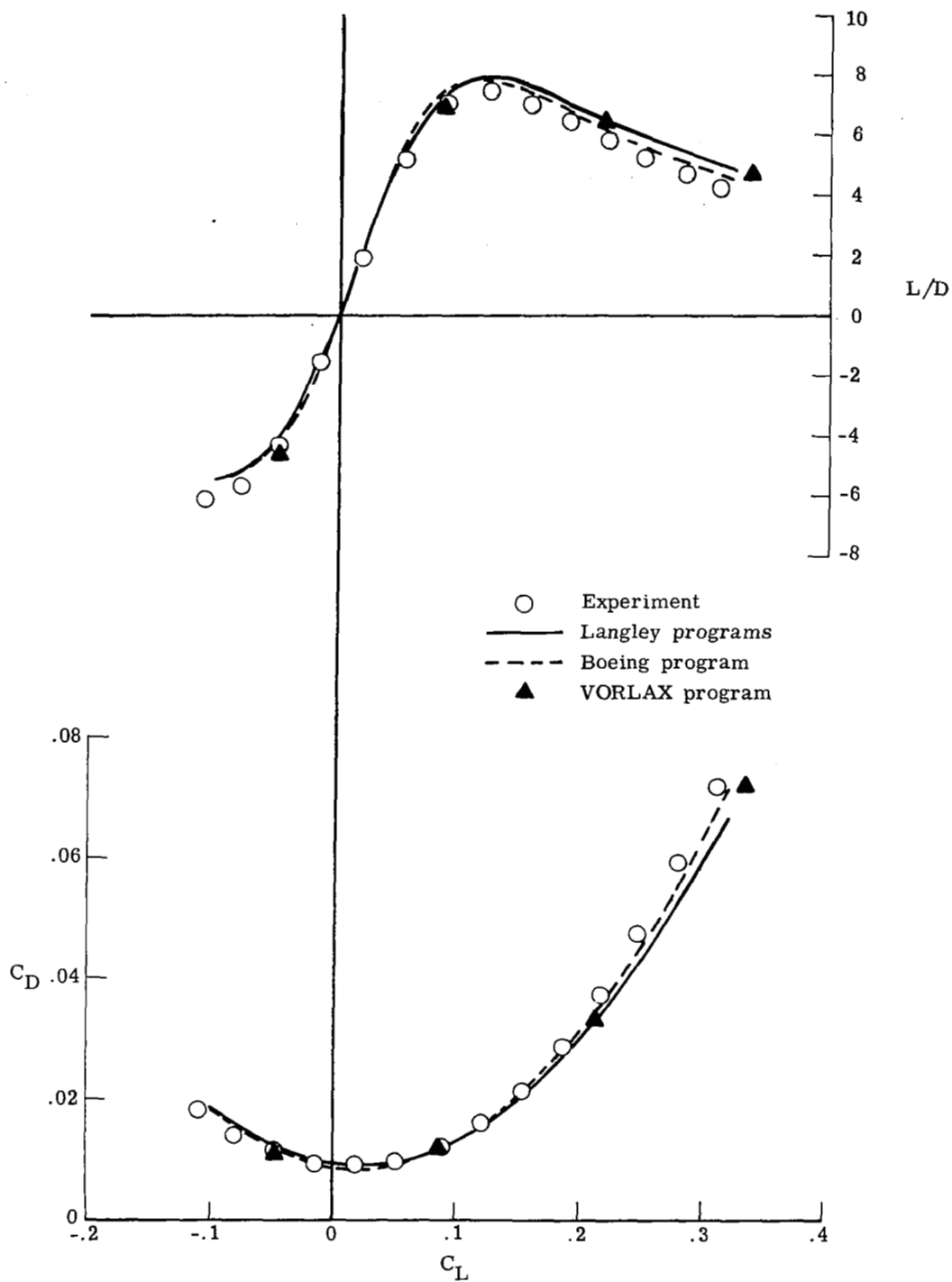
(a) Concluded.

Figure 6.- Continued.



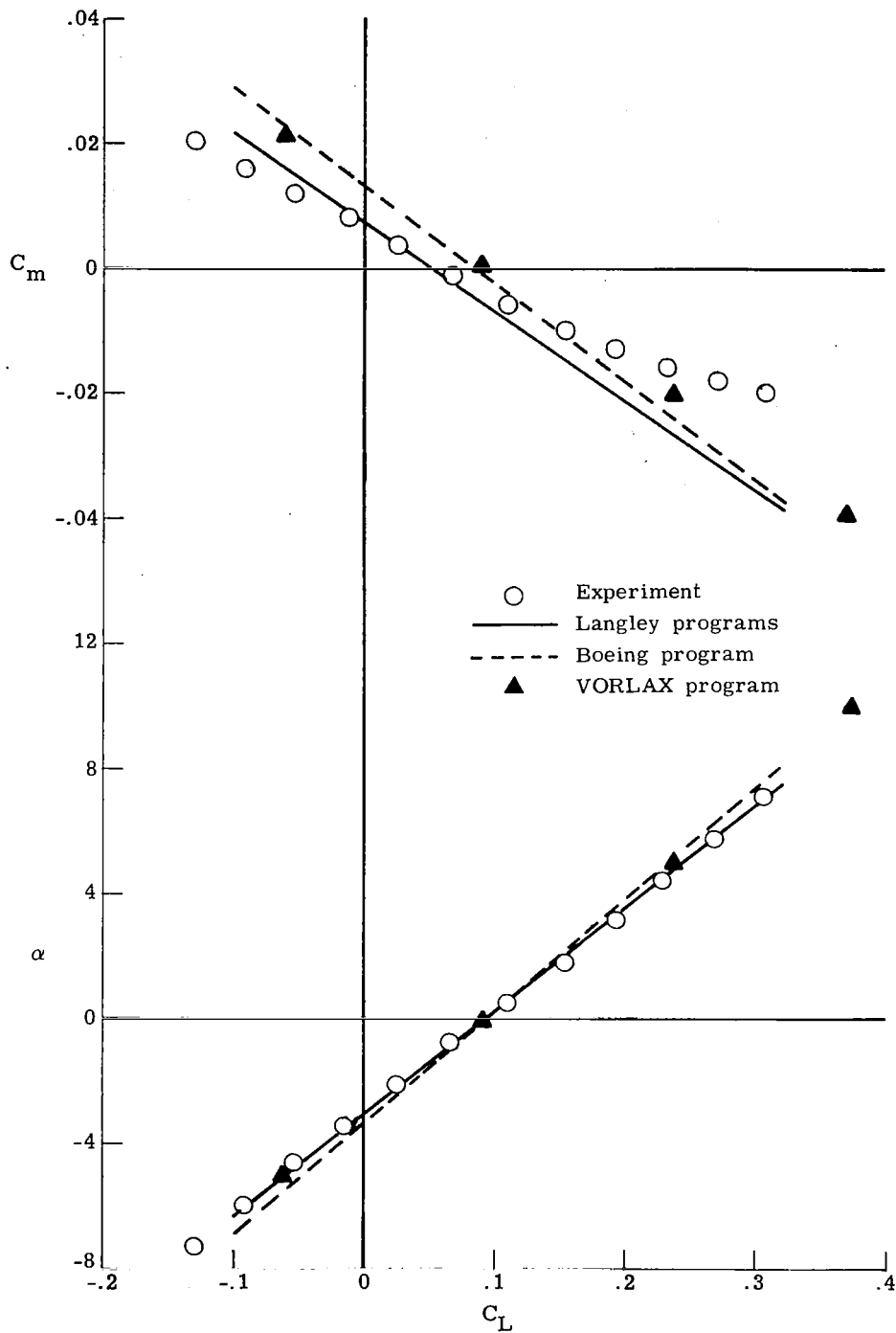
(b) $M = 2.70$.

Figure 6.- Continued.



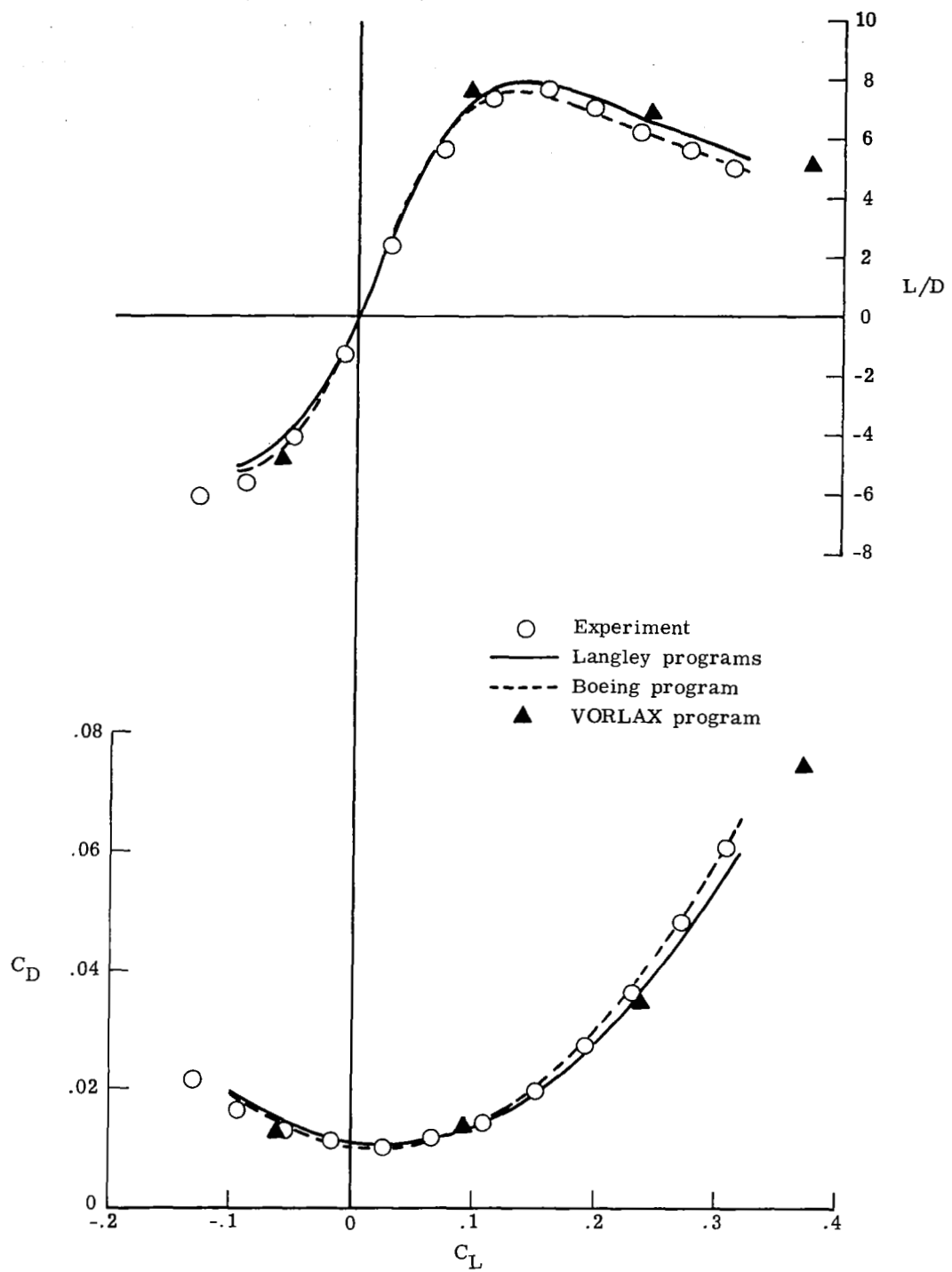
(b) Concluded.

Figure 6.- Concluded.



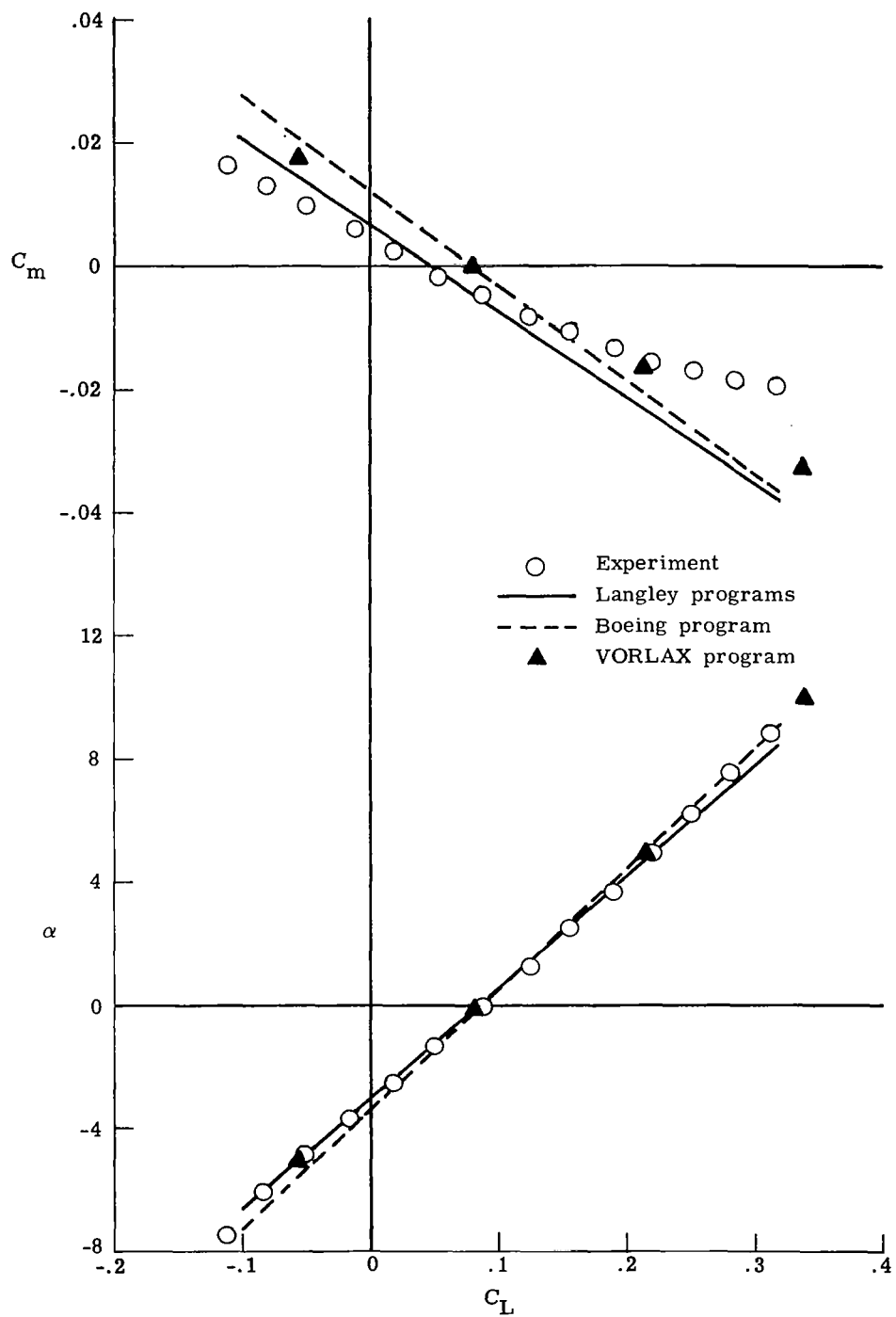
(a) $M = 2.30$.

Figure 7.- Comparison of theoretical and experimental results for complete model at supersonic speeds.



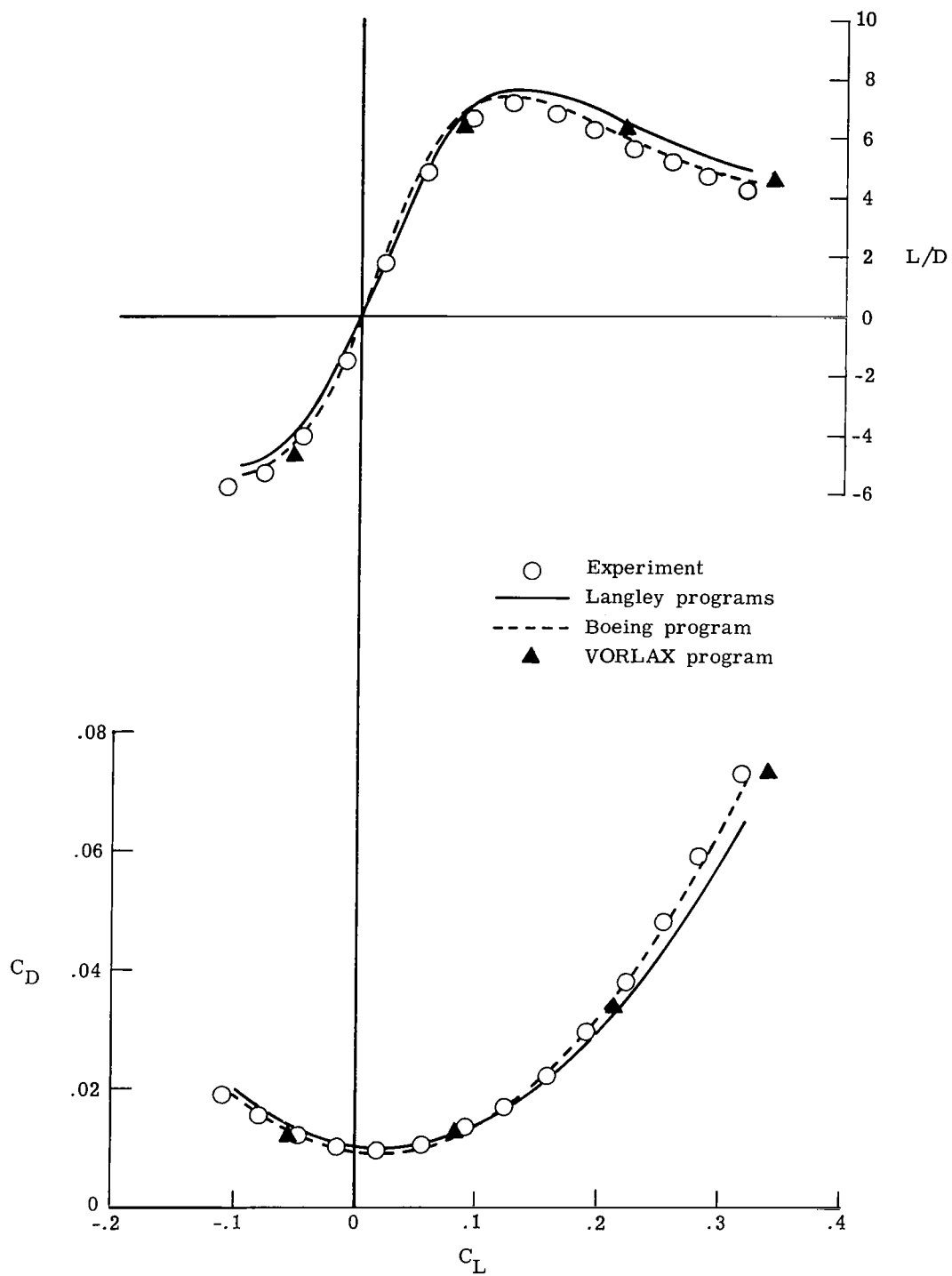
(a) Concluded.

Figure 7.- Continued.



(b) $M = 2.70$.

Figure 7.- Continued.



(b) Concluded.

Figure 7.- Concluded.

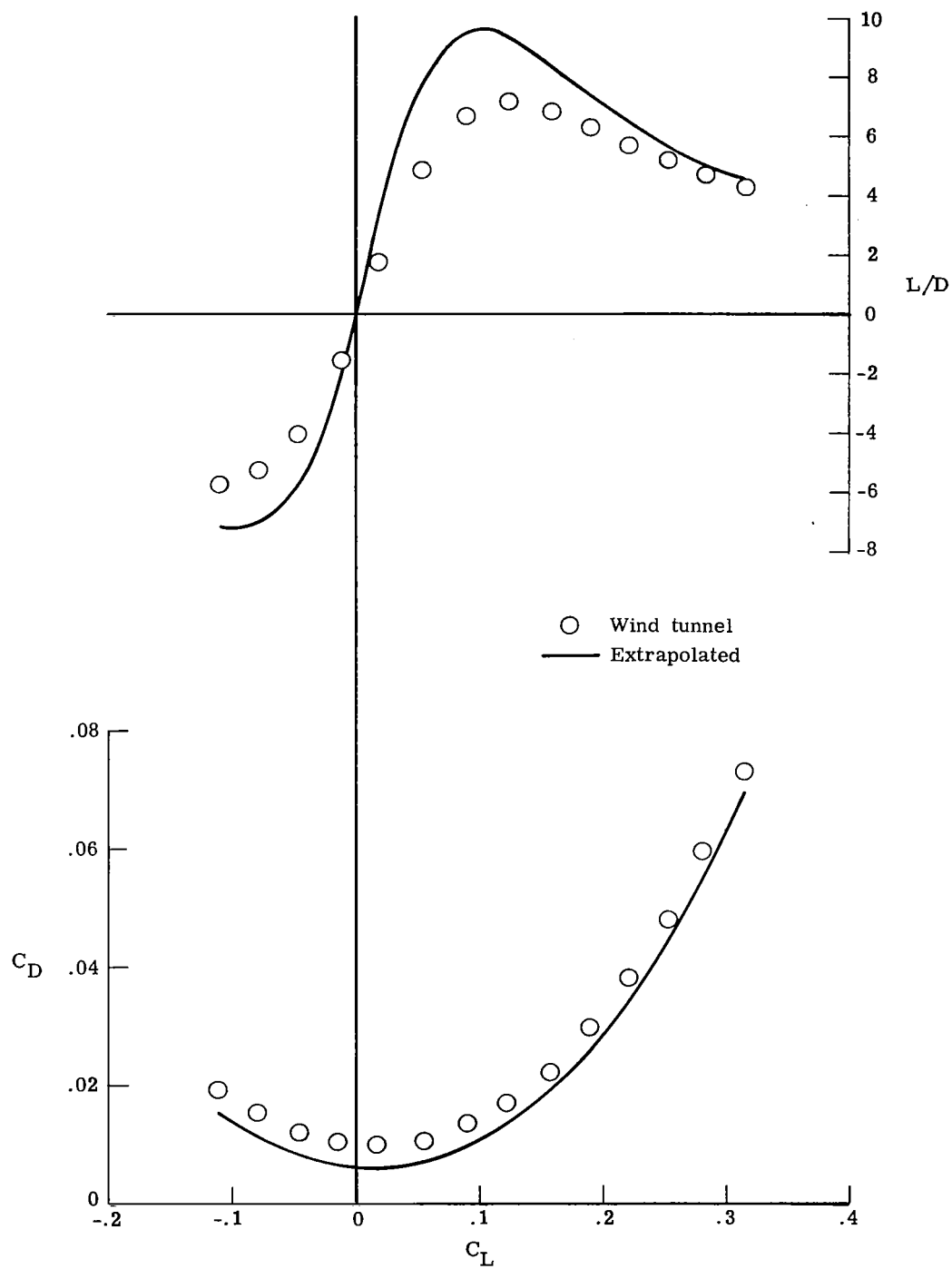


Figure 8.- Extrapolation of wind-tunnel data to full-scale flight conditions at Mach 2.70 and an altitude of 18 288 m (60 000 ft).

Figure 9.- AST-105 configuration. Dimensions in m (ft) unless otherwise noted.

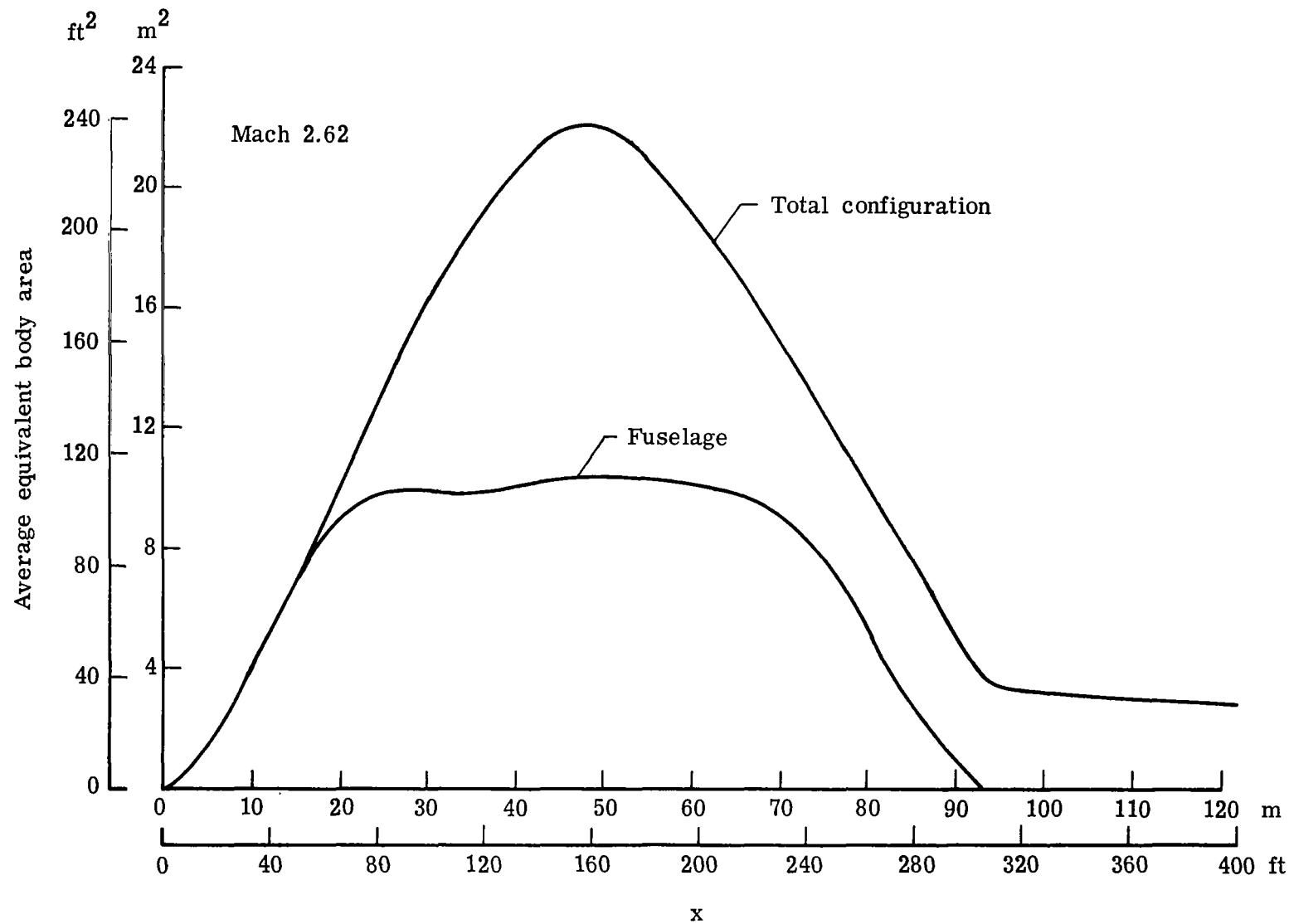


Figure 10.- Equivalent-body area distributions for AST-105 configuration.

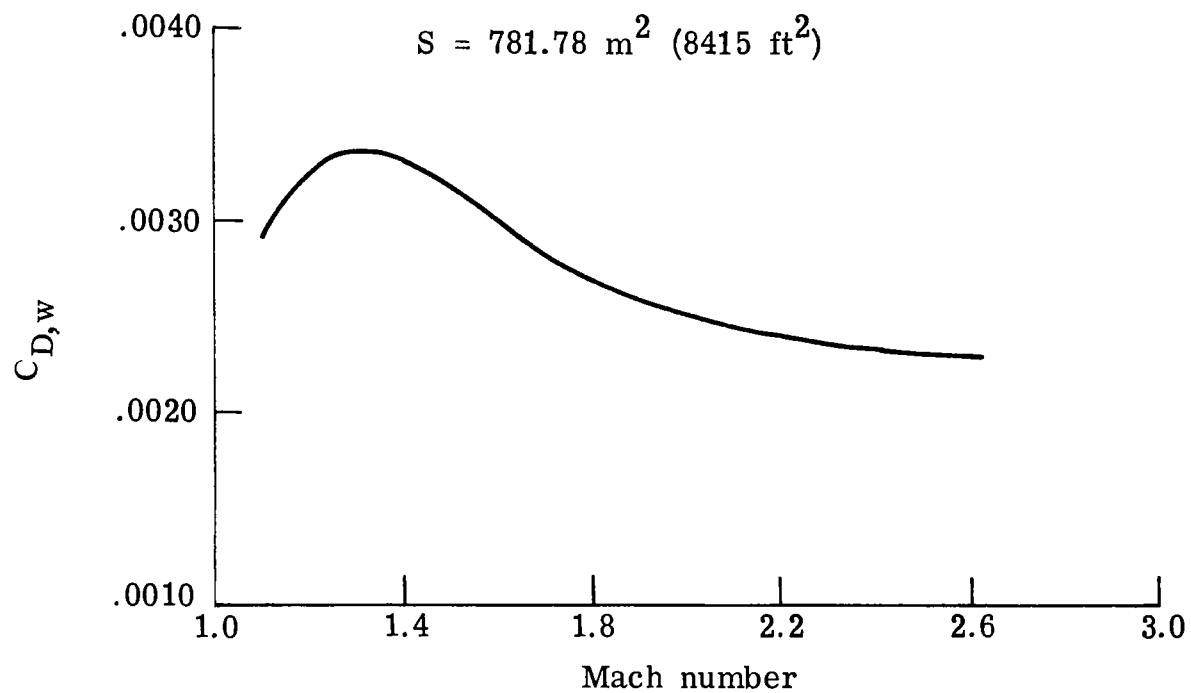


Figure 11.- Wave-drag characteristics of AST-105 configuration.

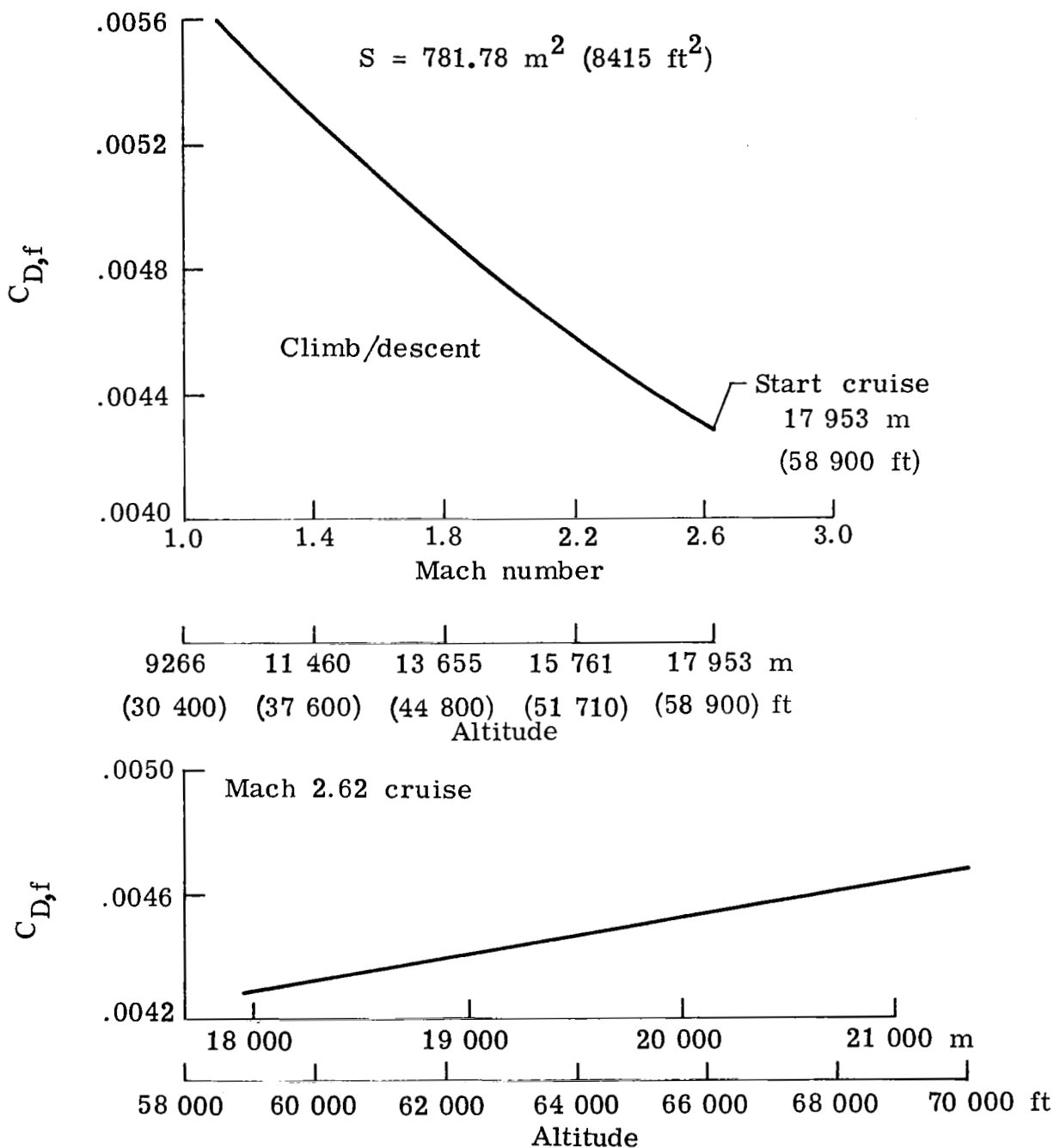


Figure 12.- Skin-friction-drag analysis for AST-105 configuration.

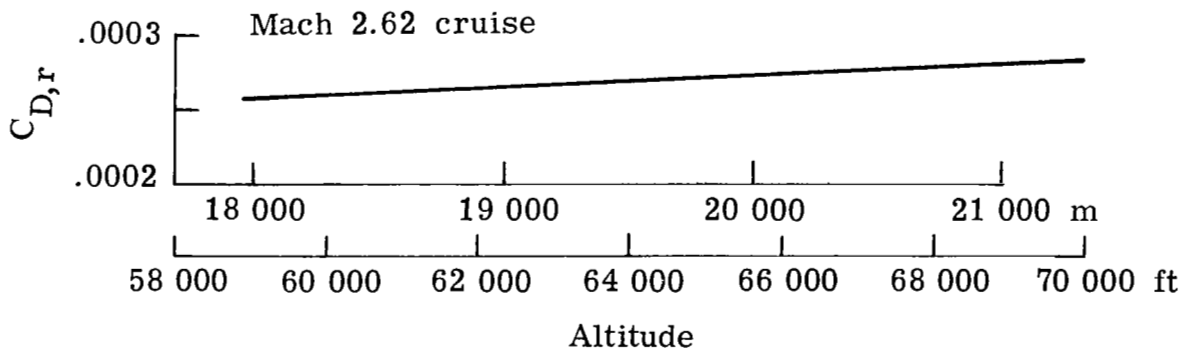
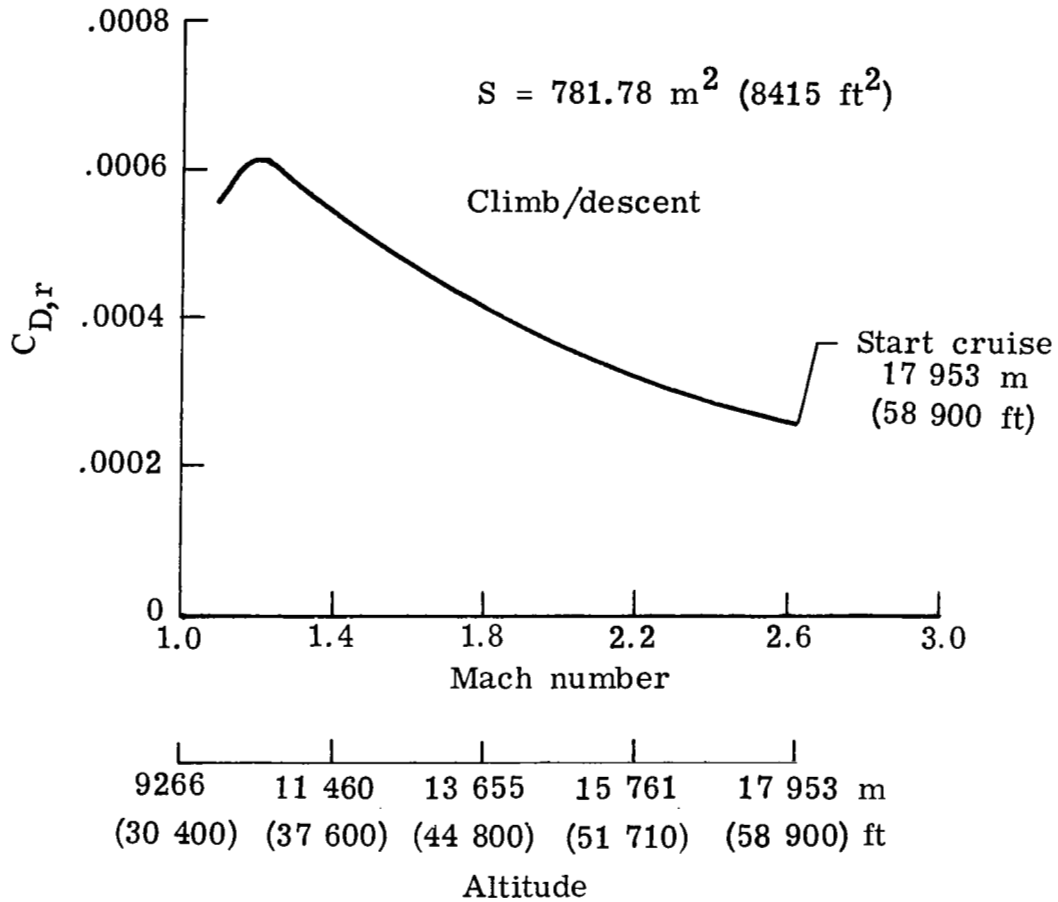


Figure 13.- Roughness-drag analysis for AST-105 configuration.

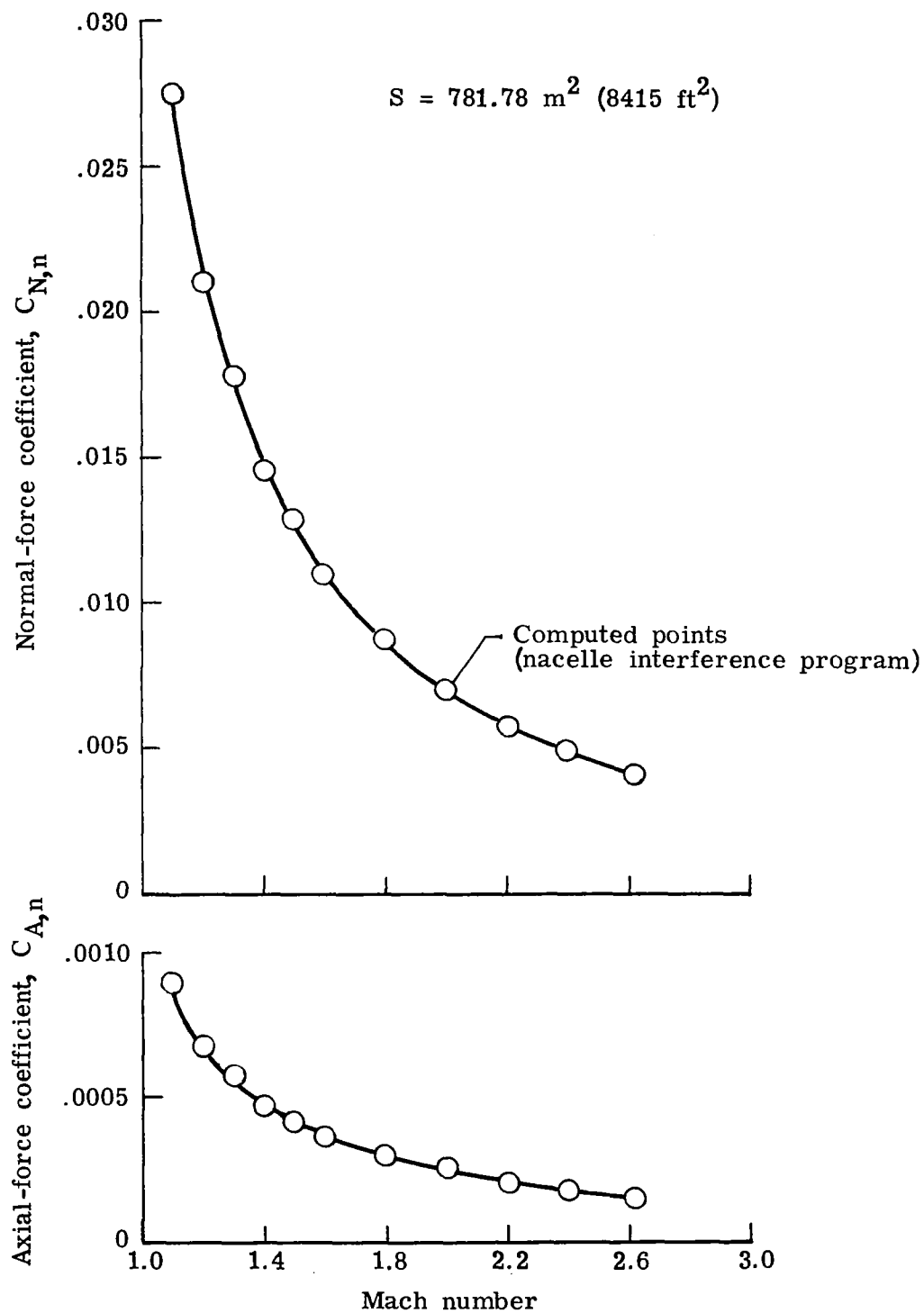


Figure 14.- Nacelle-on-wing interference for AST-105 configuration.

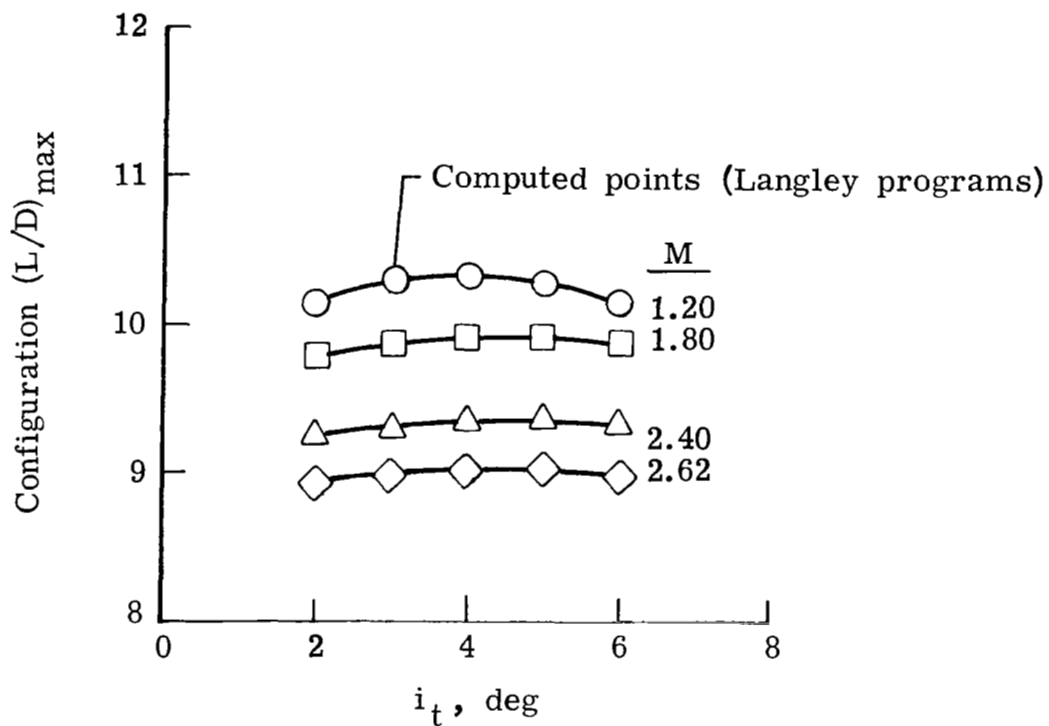


Figure 15.- Examples of AST-105 configuration performance dependence on horizontal-tail incidence.

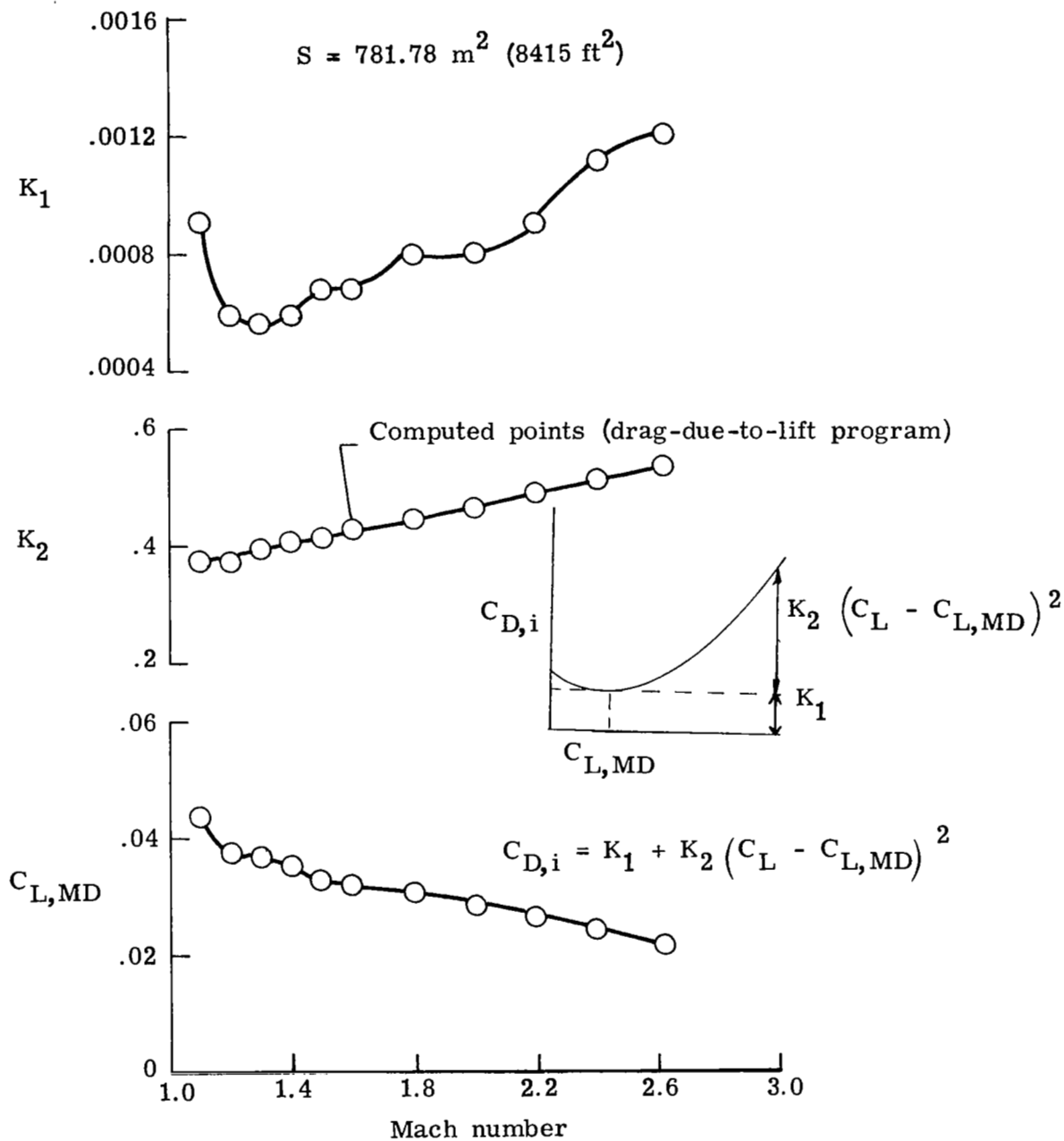


Figure 16.- Drag-due-to-lift parameters for AST-105 configuration.

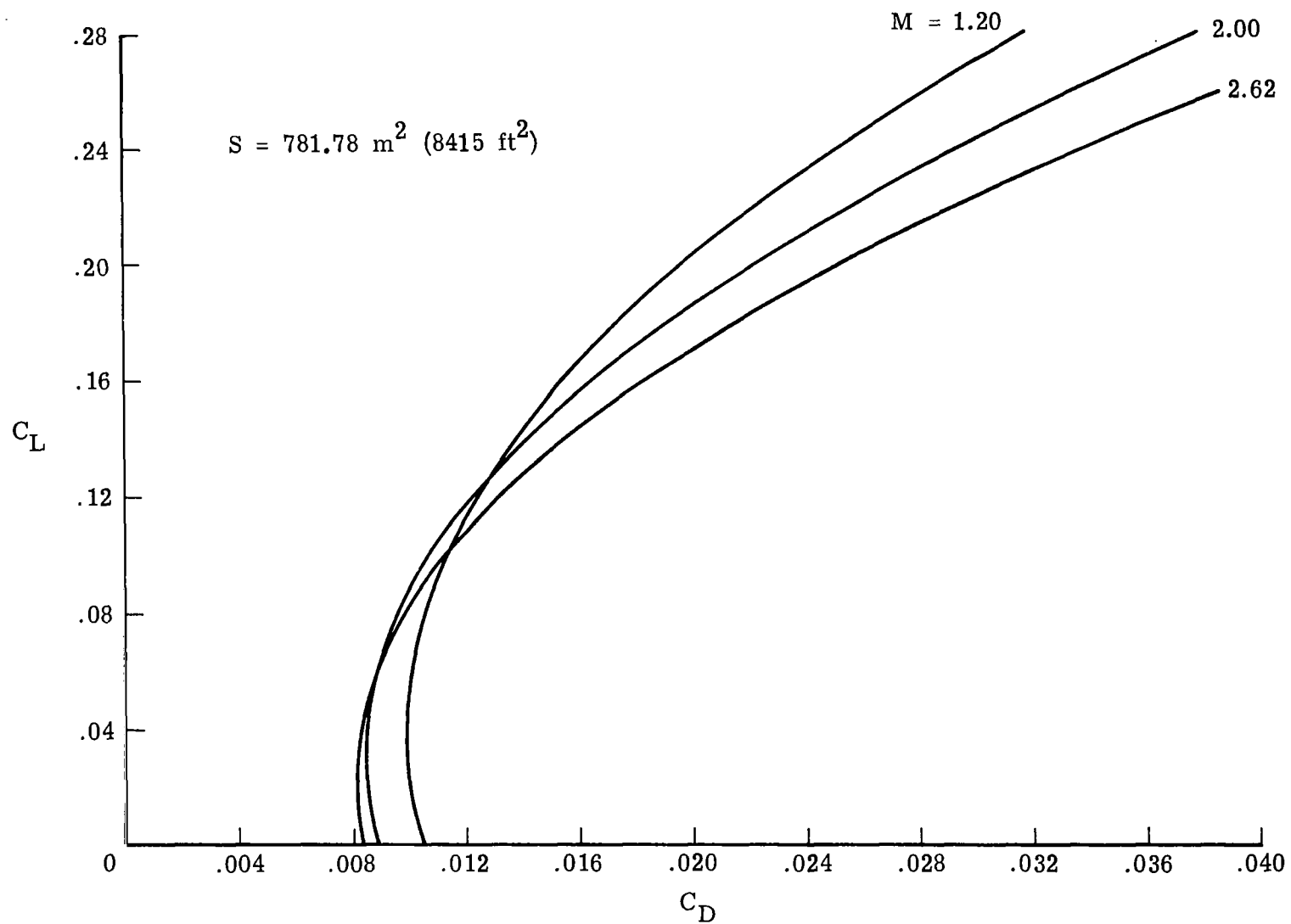


Figure 17.- Typical drag polars for AST-105 configuration.

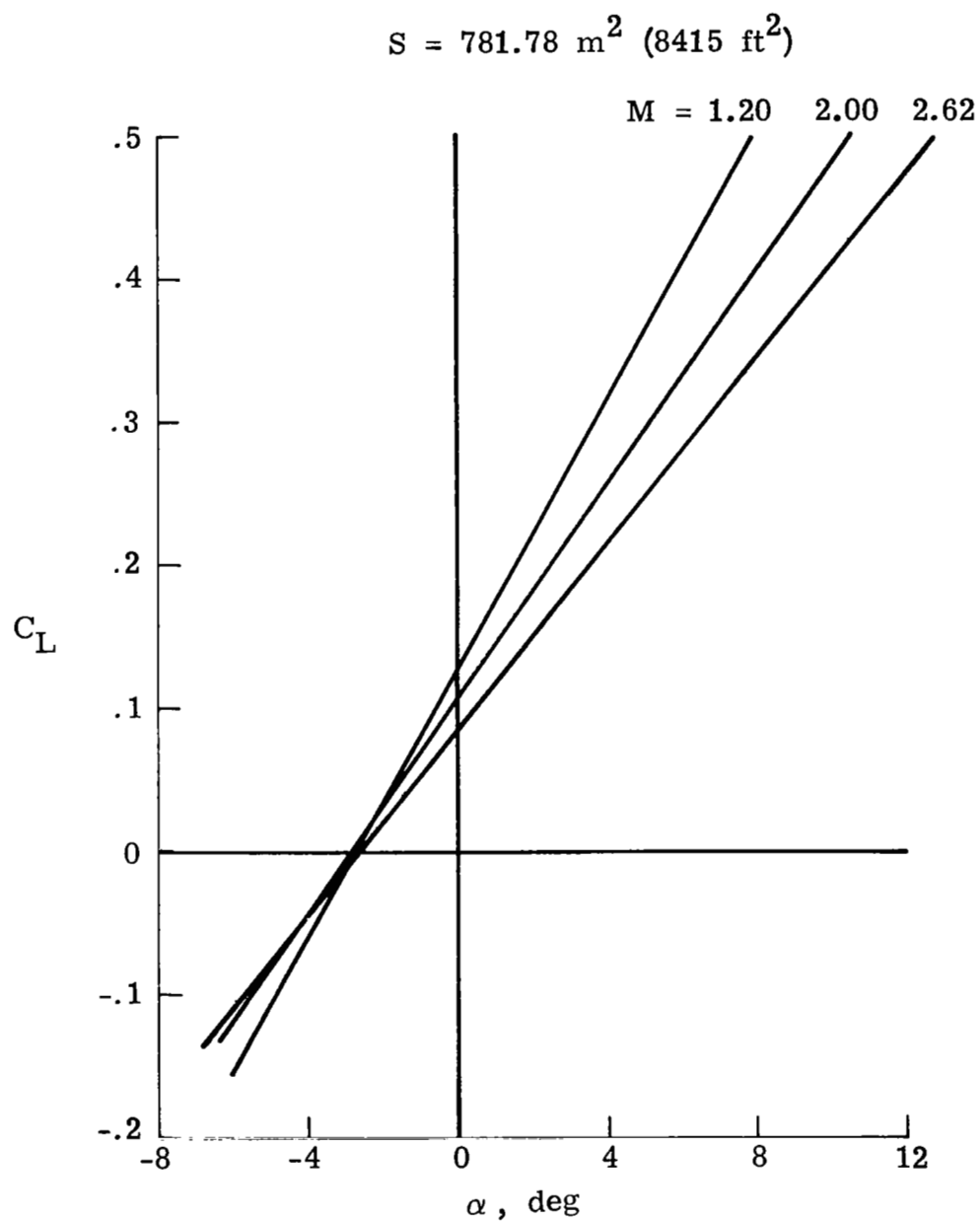


Figure 18.- Typical lift curves for AST-105 configuration.

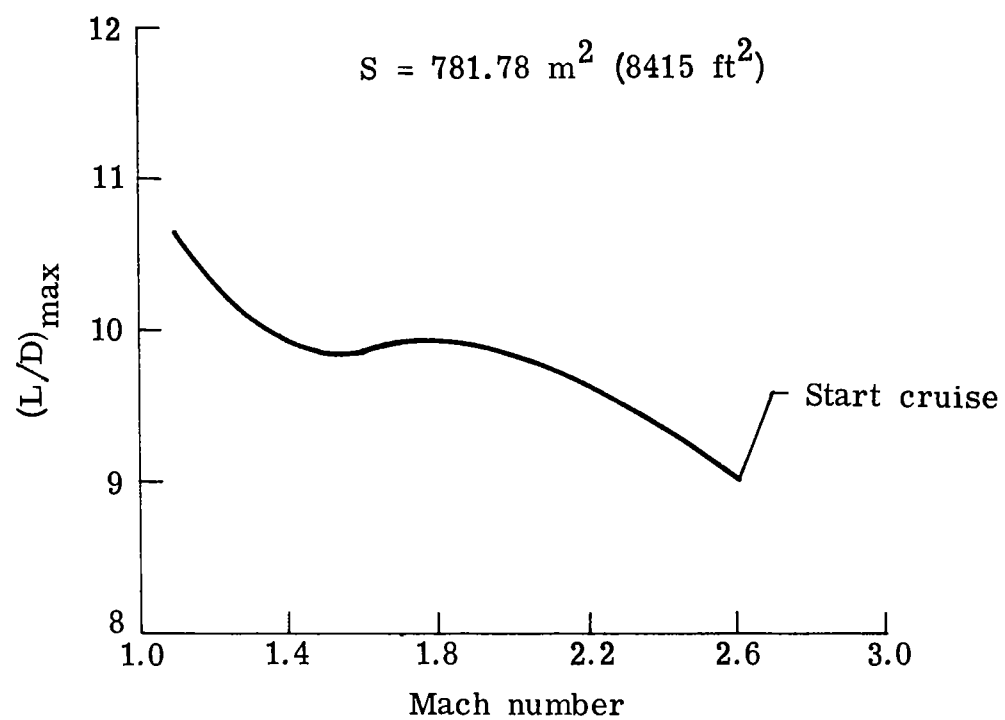


Figure 19.- $(L/D)_{\max}$ performance variation with Mach number for AST-105 configuration.

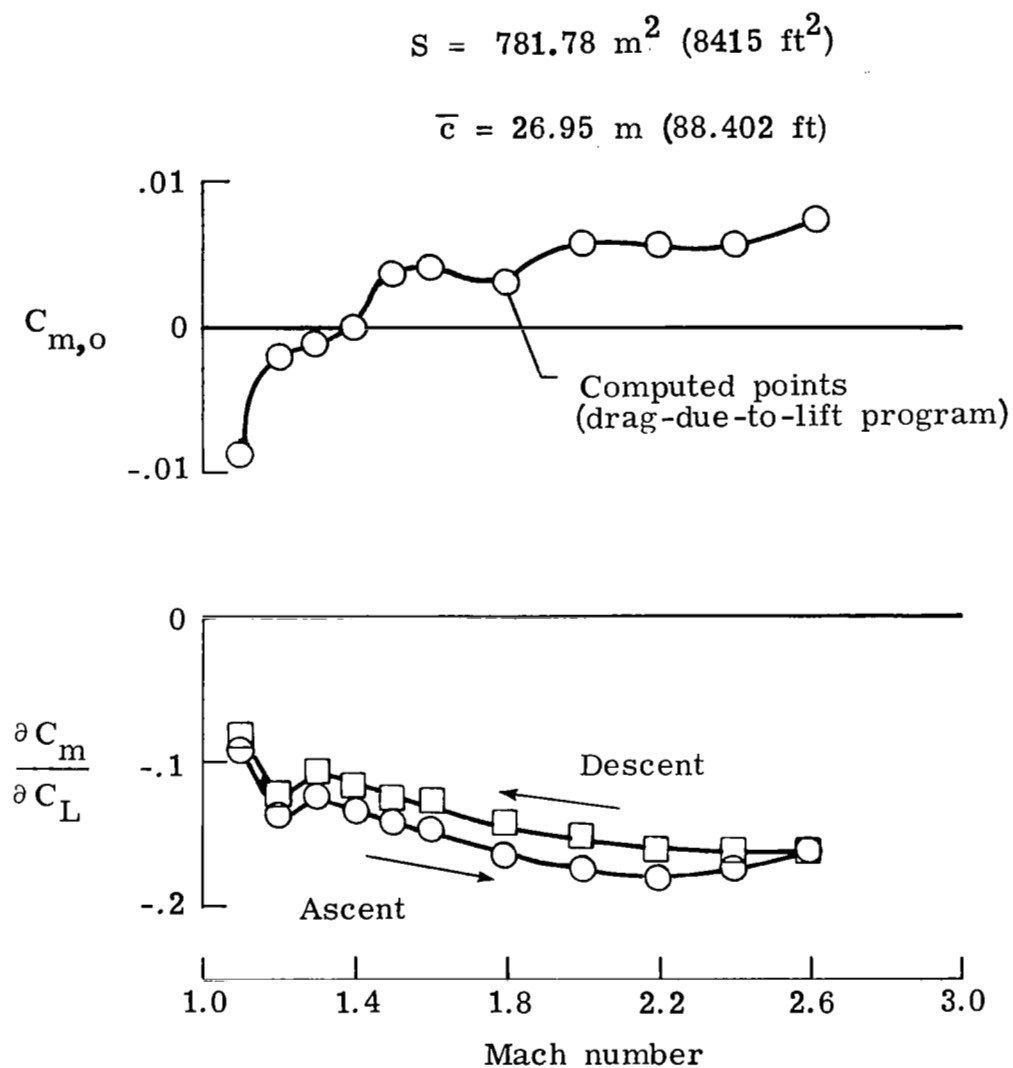


Figure 20.- Pitching-moment characteristics for AST-105 configuration.

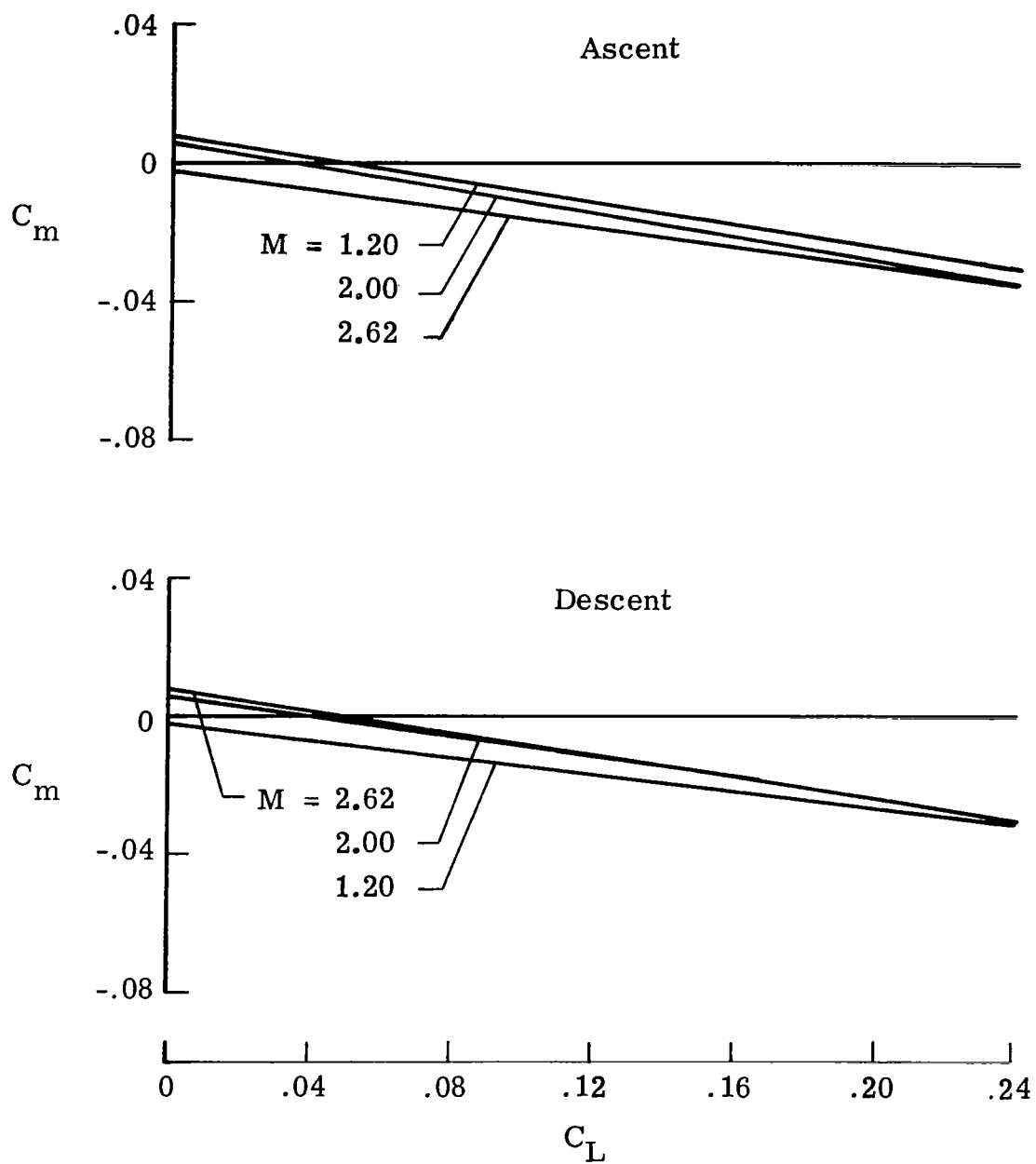


Figure 21.- Typical pitching-moment curves for AST-105 configuration.

1. Report No. NASA TP-1358		2. Government Accession No.		3. Recipient's Catalog No.	
4. Title and Subtitle THEORETICAL EVALUATION OF HIGH-SPEED AERODYNAMICS FOR ARROW-WING CONFIGURATIONS				5. Report Date January 1979	
				6. Performing Organization Code	
7. Author(s) Samuel M. Dollyhigh				8. Performing Organization Report No. L-12485	
9. Performing Organization Name and Address NASA Langley Research Center Hampton, VA 23665				10. Work Unit No. 517-53-43-01	
				11. Contract or Grant No.	
12. Sponsoring Agency Name and Address National Aeronautics and Space Administration Washington, DC 20546				13. Type of Report and Period Covered Technical Paper	
				14. Sponsoring Agency Code	
15. Supplementary Notes Analytical support in calculating lifting characteristics and the AST-105 data package were provided by Kenneth B. Walkley of Vought Corporation, Hampton Technical Center, Hampton, Va.					
16. Abstract A limited study of the use of theoretical methods to calculate the high-speed aerodynamic characteristics of arrow-wing supersonic cruise configurations has been conducted. The study included correlations of theoretical predictions with wind-tunnel data at Mach numbers from 0.8 to 2.7, examples of the use of theoretical methods to extrapolate the wind-tunnel data to full-scale flight condition, and presentation of a typical supersonic data package for an advanced supersonic transport application prepared using the theoretical methods. A brief description of the methods and their application is given.					
17. Key Words (Suggested by Author(s)) Theoretical aerodynamics Supersonic cruise vehicles			18. Distribution Statement Unclassified - Unlimited Subject Category 02		
19. Security Classif. (of this report) Unclassified	20. Security Classif. (of this page) Unclassified	21. No. of Pages 64	22. Price* \$5.25		

National Aeronautics and
Space Administration

Washington, D.C.
20546

Official Business

Penalty for Private Use, \$300

THIRD-CLASS BULK RATE

Postage and Fees Paid
National Aeronautics and
Space Administration
NASA-451



7 1 10, A, 121878 S00903DS
DEPT OF THE AIR FORCE
AF WEAPONS LABORATORY
ATTN: TECHNICAL LIBRARY (SUL)
KIRTLAND AFB NM 87117

NASA

S

POSTMASTER:

If Undeliverable (Section 158
Postal Manual) Do Not Return